

Efficient construction of \mathbb{Z}_2 gauge-invariant bases for the Quantum Minimally Entangled Typical Thermal States algorithm

Reita Maeno^{1,2,*}

¹*Department of Physics, Graduate School of Science,
The University of Tokyo, Tokyo 113-0033, Japan*

²*Yukawa Institute for Theoretical Physics, Kyoto University,
Kitashirakawa Oiwakecho, Sakyo-ku, Kyoto 606-8502 Japan*

(Dated: March 12, 2026)

In quantum computations of gauge theories at finite temperature and finite density, it is challenging to enforce Gauss's law for all states contributing to the thermal ensemble. While various techniques for implementing gauge constraints have been proposed, they often involve practical trade-offs. In this work, we adopt the Quantum Minimally Entangled Typical Thermal States (QMETTS) algorithm for \mathbb{Z}_2 gauge-constrained systems, which allows us to capture thermal equilibrium states with chemical potential while mitigating these trade-offs. To ensure that gauge invariance is preserved throughout the procedure while maintaining computational efficiency, we derive the specific measurement bases within the algorithm. Furthermore, since the estimation of expectation values on quantum hardware is inherently noisy, we rigorously account for shot noise in estimating expectation values, and propose a sampling method that is more efficient than those in previous works. We validate our approach numerically by studying a $(1+1)$ -dimensional \mathbb{Z}_2 gauge theory coupled to staggered fermions. Our proposed algorithm reproduces the correct equilibrium states at finite-temperature and finite-density.

I. INTRODUCTION

Understanding the properties of equilibrium systems at finite-temperature and finite-density in gauge theories is a central issue in modern theoretical physics, as it elucidates the physics of neutron stars, heavy-ion collisions, and the phase structure of quantum chromodynamics (QCD) [1–3]. Ab-initio numerical studies of gauge theories are among the most powerful tools for investigating such phenomena, and lattice gauge theory provides a natural framework for this purpose through lattice regularization [4, 5]. Conventional Monte Carlo studies of lattice gauge theories based on the Euclidean Lagrangian formalism have achieved remarkable success in reproducing a wide range of nonperturbative phenomena [6, 7]. However, at finite density or in real-time dynamics, these approaches suffer from the notorious sign problem, which severely limits their applicability [8]. This difficulty constitutes a major obstacle to the first-principles study of phase diagrams in QCD and related gauge theories.

Recent advances in quantum computing and quantum simulation offer a promising route to overcome these limitations. Quantum simulators enable the direct implementation of Hamiltonian dynamics without directly encountering the exponential growth of the Hilbert space, allowing for the simulation of gauge theories beyond the reach of classical

Monte Carlo methods. Nevertheless, the preparation of thermal states on quantum devices remain a challenging task as quantum simulation is naturally tailored to pure states and unitary time evolution, while thermal equilibrium states are described by Gibbs states, which are mixed states defined through non-unitary imaginary-time evolution.

Quantum algorithms for finite-temperature many-body systems have been extensively studied. First, variational approaches [9, 10] aim to prepare Gibbs states using shallow circuits and few ancillary qubits, making them suitable for near-term quantum devices. However, they can suffer from optimization difficulties such as barren plateaus. While dissipative approaches [11–15] can also prepare Gibbs states, often with high accuracy, these methods typically require ancillary systems and deep circuits, which can be challenging for near-term implementations. Another category includes typicality-based methods [16–20], which estimate thermal expectation values without explicitly preparing the Gibbs state. These approaches often allow shallow circuits and minimal ancillary resources, though they provide approximate results rather than exact Gibbs states.

One promising direction for studying thermal equilibrium systems in near-term application is the Quantum Minimally Entangled Typical Thermal States (QMETTS) algorithm by Motta et al. [21]. The QMETTS algorithm is the quantum extension of the Minimally Entangled Typical Thermal States (METTS) algorithm, which is aimed for tensor network calculation proposed by White et al. [22, 23]. It

* maeno-reita916@g.ecc.u-tokyo.ac.jp

provides a practical framework for evaluating finite-temperature observables by sampling a sequence of pure states generated through imaginary-time evolution and projective measurements. Owing to the classical sampling procedure, the required quantum circuits can be kept relatively shallow, making this approach suitable for near-term noisy intermediate-scale quantum (NISQ) devices [24] as well as early fault-tolerant quantum computing regimes.

In the QMETTS algorithm, constructing measurement bases carefully is crucial for maintaining computational efficiency. In conventional quantum many-body systems, Z -basis and X -basis are known to be optimal because those bases satisfy mutually unbiasedness (Eq. 13). However, in gauge systems, the gauge symmetry must be taken into account throughout the process. Standard projective measurements using Z or X bases typically violate gauge symmetries, rendering the calculation of correct expectation values impossible.

In this work, we propose an efficient construction that satisfies these requirements by introducing special measurement bases called Mutually Unbiased Physical Bases (see Def. IV.1), which preserve the gauge invariance of collapse states while maintaining mutual unbiasedness within the physical sector. We construct these bases by leveraging the mathematical equivalence between \mathbb{Z}_2 gauge theory and the stabilizer formalism, a framework extensively developed in quantum error correction [25, 26]. By utilizing insights from the stabilizer formalism, we identify a method to construct these bases using shallow circuits. This approach overcomes several inherent limitations of conventional strategies. For instance, while a common approach is to explicitly solve the gauge constraints and work within the physical Hilbert space [27, 28], this often results in highly non-local interactions that hinder scalability and is typically restricted to $(1+1)$ -dimensional systems. Alternatively, strategies that introduce penalty terms to energetically suppress gauge-violating states [29] face difficulties, as the required strength of the penalty depends on the magnitude of the excited-state energies, which is generally unknown. Consequently, it is uncertain how such penalties affect overall accuracy and resource requirements at finite temperature. Our method provides an alternative that maintains locality and gauge invariance without the need for manual parameter tuning and can be extended to higher dimensions.

Beyond the construction of measurement bases, we propose a more sampling-efficient approach by explicitly incorporating shot noise into the estimation of expectation values of observables. While shot noise is unavoidable in practical quantum computa-

tion, most previous studies have not accounted for its effects. We derive that shot noise can play a role in reducing the auto-correlation of the Markov chain in the process of the QMETTS, leading to small variances of estimators. This methodology is not restricted to gauge theories; it provides a general enhancement applicable to any quantum simulation utilizing the QMETTS framework.

As a numerical demonstration, we apply our algorithm to the $(1+1)$ -dimensional \mathbb{Z}_2 lattice gauge theory coupled to staggered fermions and compute its finite-temperature and finite-density phase diagram. The results show that the proposed method accurately captures the thermal behavior of the system, demonstrating its effectiveness and potential applicability to more general lattice gauge theories.

The rest of this paper is organized as follows. Section II presents the setup of the $(1+1)$ -dimensional \mathbb{Z}_2 lattice gauge theory considered in this work. Sec. III briefly reviews the METTS algorithm and the QMETTS algorithm followed by proposing sampling efficient approaches. In Sec. IV, we introduce our approach to evaluating gauge-invariant expectation values at finite-temperature and finite-density using the QMETTS framework. Based on Sec. IV, Sec. V presents numerical demonstrations for the \mathbb{Z}_2 lattice gauge theory and calculates its finite-temperature and finite-density phase diagram. Finally, Sec. VI summarizes our results and discusses future perspectives.

II. MODEL

As a concrete example, we focus on $(1+1)$ -dimensional \mathbb{Z}_2 lattice gauge theory (LGT) coupled to staggered fermions, which is the simplest discrete realization of the Schwinger model [30]. Despite its minimal local Hilbert space consisting of two-level systems, this model exhibits nontrivial properties such as confinement and has been widely used as a benchmark for quantum simulations of lattice gauge theories [31, 32]. In the staggered formulation, staggered fermions at site $2n$ and $2n+1$, χ_{2n} and χ_{2n+1} , represent the two components of a Dirac spinor at site n , ψ_n . Explicitly, a Dirac fermion ψ_n is represented by

$$\frac{\psi_n}{\sqrt{a}} = \begin{pmatrix} \chi_{2n} \\ \chi_{2n+1} \end{pmatrix}, \quad (1)$$

where a denotes the lattice spacing. In this formulation, staggered fermions reside on lattice sites and gauge fields live on the links between neighboring sites. An annihilation (creation) operator of the staggered fermion $\chi_n(\chi_n^\dagger)$ satisfies the canonical anticommutation relation $\{\chi_n, \chi_m^\dagger\} = \delta_{n,m}$. The

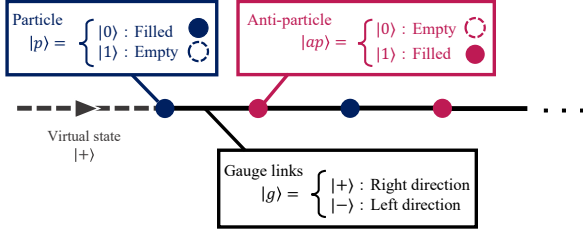


FIG. 1: Schematic setup for (1 + 1)-dimensional \mathbb{Z}_2 LGT coupled to staggered fermions. Occupied sites correspond to $|0\rangle$ ($|1\rangle$) on particle (antiparticle) sites, while empty sites correspond to $|1\rangle$ ($|0\rangle$), respectively. For gauge links, $|+\rangle$ represents right directional flux and $|-\rangle$ represents left. As boundary condition, we impose open boundary condition and set right-directional flux $|+\rangle$ with the most left site.

Hamiltonian is given by

$$H = \frac{1}{2a} \sum_{n=1}^{L_{\text{KS}}-1} [\chi_n^\dagger \sigma_{n,n+1}^Z \chi_{n+1} + \text{h.c.}] + ag^2 \sum_{n=1}^{L_{\text{KS}}-1} [1 - \sigma_{n,n+1}^X] + m \sum_{n=1}^{L_{\text{KS}}} (-1)^n \chi_n^\dagger \chi_n, \quad (2)$$

where g, m are gauge coupling, and fermion mass, respectively. $\sigma_{n,n+1}^Z$ and $\sigma_{n,n+1}^X$ are Pauli operators in the \mathbb{Z}_2 link and electric field operators, respectively. As we noted, lattice sites reproducing Dirac fermion L_D has half lattice sites compared with staggered one L_{KS} , $L_D = L_{\text{KS}}/2$.

After mapping fermionic degrees of freedom into spin operators via Jordan-Wigner transformation [33], the qubit description of the Hamiltonian is given in the following form;

$$H = -\frac{1}{4a} \sum_{n=1}^{L_{\text{KS}}-1} [X_n \sigma_{n,n+1}^Z X_{n+1} + Y_n \sigma_{n,n+1}^Z Y_{n+1}] + ag^2 \sum_{n=1}^{L_{\text{KS}}-1} [1 - \sigma_{n,n+1}^X] + \frac{m}{2} \sum_{n=1}^{L_{\text{KS}}} (-1)^n Z_n, \quad (3)$$

where X_n, Y_n , and Z_n are usual Pauli matrices acting on the qubit at site n . In this representation, as shown in Fig. 1, the qubit basis is defined as follows. On odd sites, which correspond to particle states, $|0\rangle$ ($|1\rangle$) corresponds to an occupied (empty) fermionic state, whereas on even (antiparticle) sites, $|1\rangle$ ($|0\rangle$) represents an occupied (empty) state. For gauge links, $|+\rangle$ ($|-\rangle$) represents right (left) directional flux. We impose the open boundary condition where the most left particle state connect with the state $|+\rangle$ from the left virtual link.

In addition, gauge theories must respect local gauge symmetries, inducing conservation laws called Gauss's laws. In our setup, Gauss's law operators are represented by

$$G_n = (-1)^n \sigma_{n-1,n}^X Z_n \sigma_{n,n+1}^X \quad (1 \leq n \leq L_{\text{KS}} - 1). \quad (4)$$

Due to the boundary condition, we fix $\sigma_{0,1}^X = 1$. Their eigenvalues are $g_n = \pm 1$. They commute with each other, $[G_n, G_m] = 0$, $\forall n, m$ and with Hamiltonian $[H, G_n] = 0$, $\forall n$. In this work, we choose a sector without background, called physical sector, which is realized $g_n = 1$, $\forall n$. Once we fix sector to physical sector, the states contributing to expectation values are only physical states $|\psi\rangle$ satisfying $G_n |\psi\rangle = +|\psi\rangle$, $\forall n$. We denote subspace spanned by physical states as $\mathcal{H}_{\text{phys}}$ and total Hilbert space as \mathcal{H}_{tot} . Enforcing this constraint poses a nontrivial challenge for computation of gauge theories.

To study thermal-equilibrium properties of the theory, we consider the calculation of grand-canonical ensemble of an observable \mathcal{O} under inverse temperature $\beta = 1/T$ and chemical potential μ :

$$\langle \mathcal{O} \rangle_{\beta, \mu} := \text{Tr}_{\mathcal{H}_{\text{phys}}} \left[\mathcal{O} \frac{e^{-\beta(H - \mu N)}}{Z} \right], \quad (5)$$

where N is the number operator given by

$$N = \sum_{n=1}^{L_{\text{KS}}} \chi_n^\dagger \chi_n = \frac{1}{2} \sum_{n=1}^{L_{\text{KS}}} Z_n. \quad (6)$$

Note that trace is taken over only physical subspace $\mathcal{H}_{\text{phys}}$. Since the number operator N commutes with all Gauss's law operators G_n , the grand-canonical ensemble is compatible with gauge invariance.

III. METTS / QMETTS ALGORITHM

In this section, we review and discuss the Minimally Entangled Typical Thermal States (METTS) algorithm and its quantum counterpart, known as the Quantum Minimally Entangled Typical Thermal States (QMETTS) algorithm. The METTS algorithm was first proposed by White et al. [22, 23] in the context of tensor network approaches. Subsequently, Motta et al. [21] extended this framework to quantum computing, developing the QMETTS algorithm. Both approaches serve as key methodologies for calculating expectation values of an observable at finite-temperature and finite-density in quantum many-body systems. We begin with a brief review of the METTS approach, followed by a detailed discussion of the QMETTS algorithm. In the subsection

dedicated to QMETTS, we propose a more efficient sampling method that accounts for shot noise, offering an improved approach for precise estimations of expectation values over previous studies. Note that this section focuses on the algorithms without gauge constraints; these constraints will be incorporated into our modified scheme in Sec. IV.

A. METTS algorithm

To explain the METTS algorithm, we rewrite the expectation value $\langle \mathcal{O} \rangle_{\beta, \mu} = \text{Tr}[\mathcal{O} e^{-\beta(H - \mu N)} / Z]$ in terms of an orthonormal basis $\{|n\rangle\}$

$$\langle \mathcal{O} \rangle_{\beta, \mu} = \sum_{|i\rangle \in \{|n\rangle\}} \frac{1}{Z} \langle i | e^{-\beta(H - \mu N)/2} \mathcal{O} e^{-\beta(H - \mu N)/2} | i \rangle \quad (7)$$

$$= \sum_{|i\rangle \in \{|n\rangle\}} \text{Prob}_i \cdot \langle \phi_i | \mathcal{O} | \phi_i \rangle, \quad (8)$$

where $|\phi_i\rangle = e^{-\beta(H - \mu N)/2} |i\rangle / \sqrt{\langle i | e^{-\beta(H - \mu N)} |i\rangle}$ and $\text{Prob}_i = \langle i | e^{-\beta(H - \mu N)} |i\rangle / Z$. Since $|\phi_i\rangle$ is normalized, it represents a pure quantum state, and Prob_i forms a probability distribution satisfying $\text{Prob}_i \geq 0$ and $\sum_i \text{Prob}_i = 1$. If we take $\{|n\rangle\}$ as a product basis, $|\phi_i\rangle$ typically has low entanglement. For this reason, the states $|\phi_i\rangle$ are referred to as Minimally Entangled Typical Thermal States (METTS) following Ref. [22]. Therefore, the thermal expectation value can be interpreted as an average of the expectation values under each METTS $\langle \phi_i | \mathcal{O} | \phi_i \rangle$ weighted by Prob_i .

The goal of the METTS algorithm is to sample these contributions efficiently by generating a Markov chain of $|i\rangle$ whose stationary distribution is Prob_i . First, we sample one state $|i\rangle$ from the measurement basis $\{|n\rangle\}$ and apply (normalized) imaginary-time evolution (ITE) operator $e^{-\beta(H - \mu N)/2}$ to $|i\rangle$, $|i\rangle \mapsto |\phi_i\rangle = e^{-\beta(H - \mu N)/2} |i\rangle / \sqrt{\langle i | e^{-\beta(H - \mu N)} |i\rangle}$. Next, we perform projective measurement for the METTS $|\phi_i\rangle$ with the measurement basis $\{|n\rangle\}$ and obtain a new collapse state $|i'\rangle$. By repeating the processes of the ITE and the projective measurement, one can generate the Markov chain with the stationary distribution Prob_i because the transition probability from $|i\rangle$ to $|i'\rangle$, $T_{i \rightarrow i'} := |\langle i' | \phi_i \rangle|^2$, holds the detailed balanced condition:

$$\frac{T_{i \rightarrow i'}}{T_{i' \rightarrow i}} = \frac{\langle i' | e^{-\beta(H - \mu N)} |i\rangle}{\langle i | e^{-\beta(H - \mu N)} |i'\rangle} = \frac{\text{Prob}_{i'}}{\text{Prob}_i}. \quad (9)$$

We generate a Markov chain of length N_{chain} , which produces a sequence of sampled METTS

$\{|\phi_{i_k}\rangle\}_{k=1}^{N_{\text{chain}}}$. For each generated METTS $|\phi_{i_k}\rangle$ we compute the observable estimate $\mu_k = \langle \phi_{i_k} | \mathcal{O} | \phi_{i_k} \rangle$ in parallel. Defining the Monte Carlo average $\bar{\mu} = (1/N_{\text{chain}}) \sum_{k=1}^{N_{\text{chain}}} \mu_k$, this estimator satisfies

$$\mathbb{E}[\bar{\mu}] = \frac{1}{N_{\text{chain}}} \sum_k \mathbb{E}[\mu_k] = \langle \mathcal{O} \rangle_{\beta, \mu}. \quad (10)$$

Thus, in the limit of large N_{chain} , the Monte Carlo average converges to the thermal expectation value.

Regarding the statistical error of the Markov chain, we must account for the auto-correlations between successive samples. Let τ_μ denote the integrated auto-correlation time for the sequence of $\{\mu_k\}_{k=1}^{N_{\text{chain}}}$. For a sufficiently long Markov chain, the variance of the the Monte Carlo average $\bar{\mu}$ is then given by [34–36],

$$\text{Var}[\bar{\mu}] = \frac{2\tau_\mu}{N_{\text{chain}}} \sigma_\mu^2, \quad (11)$$

where $\sigma_\mu^2 = \sum_i \text{Prob}_i \cdot \mu_i^2 - (\sum_i \text{Prob}_i \cdot \mu_i)^2$ represents the variance of μ_i with respect to the METTS distribution Prob_i . This relation implies that the Markov chain effectively yields $N_{\text{eff}} = N_{\text{chain}}/2\tau_\mu$ independent samples. The integrated auto-correlation time τ_μ is defined by

$$\tau_\mu = \frac{1}{2} + \sum_{t=1}^{\infty} \rho_\mu(t), \quad \rho_\mu(t) = \frac{\text{Cov}(\mu_k, \mu_{k+t})}{\sigma_\mu^2}, \quad (12)$$

where $\rho_\mu(t)$ is the normalized auto-correlation function. This function quantifies the degree of correlation between samples. For a sequence of completely independent samples, $\rho_\mu(t) = 0$, resulting in $\tau_\mu = 1/2$.

In practice, as discussed in Refs. [22, 37, 38], however, it is not efficient to consider only a single measurement basis because it does not ensure ergodicity and causes a long auto-correlation length of the chain. To make the algorithm efficient, one needs to use two bases and alternate the measurement bases. Considering the behavior of the imaginary time operator near the infinite-temperature limit ($\beta = 0$), $e^{-\beta(H - \mu N)/2} \approx I$, the measurement bases $\{|n^{(1)}\rangle\}$ and $\{|m^{(2)}\rangle\}$ overcoming those problems should satisfy

$$|\langle i^{(1)} | j^{(2)} \rangle|^2 = \frac{1}{d}, \quad (13)$$

for each state $|i^{(1)}\rangle \in \{|n^{(1)}\rangle\}$ and $|j^{(2)}\rangle \in \{|m^{(2)}\rangle\}$, where d is the dimension of the Hilbert space [37, 38]. The most representative bases to satisfy this relation are X and Z (i.e. computational) bases. In the language of quantum information, those bases satisfying Eq. (13) are called Mutually Unbiased Bases (MUB) [39]. In summary, the efficient algorithm is following:

1. Choose one state $|i^{(1)}\rangle$ from an measurement basis $\{|n^{(1)}\rangle\}$.
2. Generate the METTS by the ITE, $|\phi_i^{(1)}\rangle = e^{-\beta(H-\mu N)/2} |i^{(1)}\rangle / \sqrt{\langle i^{(1)} | e^{-\beta(H-\mu N)} | i^{(1)} \rangle}$.
3. Compute the observable estimate of \mathcal{O} under the METTS $|\phi_i^{(1)}\rangle$; $\langle \phi_i^{(1)} | \mathcal{O} | \phi_i^{(1)} \rangle$.
4. Measure the $|\phi_i^{(1)}\rangle$ with another measurement basis $\{|m^{(2)}\rangle\}$ satisfying the condition of the MUB with $\{|n^{(1)}\rangle\}$, leading to a collapse into a basis state $|j^{(2)}\rangle \in \{|m^{(2)}\rangle\}$ with probability $|\langle j^{(2)} | \phi_i^{(1)} \rangle|^2$.
5. Repeat the same step from 2 to 4 switching the role of $\{|n^{(1)}\rangle\}$ and $\{|m^{(2)}\rangle\}$ with N_{chain} times.
6. Average the samples $\langle \phi_i^{(a)} | \mathcal{O} | \phi_i^{(a)} \rangle$ ($a = 1, 2$).

In the next subsection, we explain the quantum version of this algorithm, called the QMETTS algorithm. In addition to this, by modifying the scheme to estimate observables, we show the improvement of the sampling efficiency.

B. QMETTS algorithm and Sampling Improvements

In this section, we discuss the QMETTS algorithm and analyze an efficient strategy for estimating observables under realistic shot noise. In QMETTS, the preparation of initial states, imaginary time evolution, projective measurements, and estimation of expectation values are implemented on quantum computers. The thermal expectation values, which correspond to the Monte Carlo averages of observable estimates, are obtained by classically post-processing the measured data. Similar to the original METTS algorithm, alternating between at least two measurement bases is essential for generating an efficient Markov chain, with the MUB being the optimal choice. Unlike tensor network-based approaches, quantum computation can tolerate larger amounts of entanglement and this allows for greater flexibility in designing measurement bases although the permissible amount of entanglement is limited by hardware noise and gate fidelity in the near-term era. As demonstrated in the following sections, we propose efficient measurement bases for the QMETTS algorithm in the context of gauge theories, where the required states inevitably involve a certain degree of entanglement. In the following, we analyze how shot noise affects the estimation of observables in QMETTS and propose an improved sampling strategy.

In contrast to the tensor network methods, quantum computations inherently involve shot noise when estimating the expectation values of observables while many previous studies on the QMETTS algorithm assume that expectation values can be determined exactly, mirroring the ideal METTS framework. In a realistic scenario, each estimation of expectation values is subject to shot noise with a variance $\sigma_{\text{shot}}^2 |_{\phi_i} = \langle \phi_i | \mathcal{O}^2 | \phi_i \rangle - \langle \phi_i | \mathcal{O} | \phi_i \rangle^2$, where $\sigma_{\text{shot}}^2 |_{\phi_i}$ represents the variance under each METTS $|\phi_i\rangle$. For each state in the Markov chain, the observable expectation value is estimated using N_{shot} measurements. Thus the total number of circuit executions used for observable estimation is $N_{\text{est}} = N_{\text{chain}} N_{\text{shot}}$; see Fig. 2. The resulting sequence of observations $\{O_k\}_{k=1}^{N_{\text{chain}}}$ can be expressed as $O_k = \mu_k + \varepsilon_k$, where ε_k represents the shot noise. Note that each estimate O_k is obtained from N_{shot} measurements, $O_k = (1/N_{\text{shot}}) \sum_{l=1}^{N_{\text{shot}}} o_{k,l}$, where $o_{k,l}$ represents the outcome of the measurement for estimation of observable. Let $\bar{O} = (1/N_{\text{chain}}) \sum_{k=1}^{N_{\text{chain}}} O_k$ be the sample average. The total variance of the estimator, denoted by $\text{Var}_{\text{est}}^{(\text{multi})}[\bar{O}]$, can be evaluated by the law of the total variance,

$$\text{Var}_{\text{est}}^{(\text{multi})}[\bar{O}] = \frac{2\tau^{(\text{multi})}}{N_{\text{chain}}} \sigma_{\mu}^2 + \frac{2\tau^{(\text{multi})}}{N_{\text{chain}} N_{\text{shot}}} \sigma_{\text{shot}}^2, \quad (14)$$

where $\tau^{(\text{multi})}$ is the integrated auto-correlation time for the Markov chain when each step is estimated using N_{shot} measurements. Here, σ_{shot}^2 represents the average shot noise variance over the sampled states, $\sigma_{\text{shot}}^2 = \mathbb{E}_{\text{chain}}[\sigma_{\text{shot}}^2 |_{\phi_i}]$. If N_{shot} is sufficiently large such that shot noise becomes negligible, $\tau^{(\text{multi})}$ is well-approximated by the ideal auto-correlation time of the original Markov chain τ_{μ} .

The conventional approaches require minimizing two distinct sources of error—shot noise and Markov chain sampling noise—which typically necessitates a large number of shots. In contrast, we propose an alternative, more efficient sampling strategy: estimating the observable with only a single shot ($N_{\text{shot}} = 1$) for each basis state in the chain as represented in Fig. 2. In this case, the total number of circuit executions for estimating observables equals the chain length ($N_{\text{est}} = N_{\text{chain}}$). Below, we demonstrate that this single-shot approach not only converges to the correct thermal expectation value but also reduces the total variance of the estimator under the fixed number of circuits used for observable estimation. First, the convergence is guaranteed by the law of total expectation:

$$\mathbb{E}_{\text{est}}[\bar{O}] = \mathbb{E}_{\text{chain}}[\mathbb{E}_{\text{shot}}[\bar{O}]] = \langle \mathcal{O} \rangle_{\mu, \beta}. \quad (15)$$

Next, the total variance of the single-shot estimator,

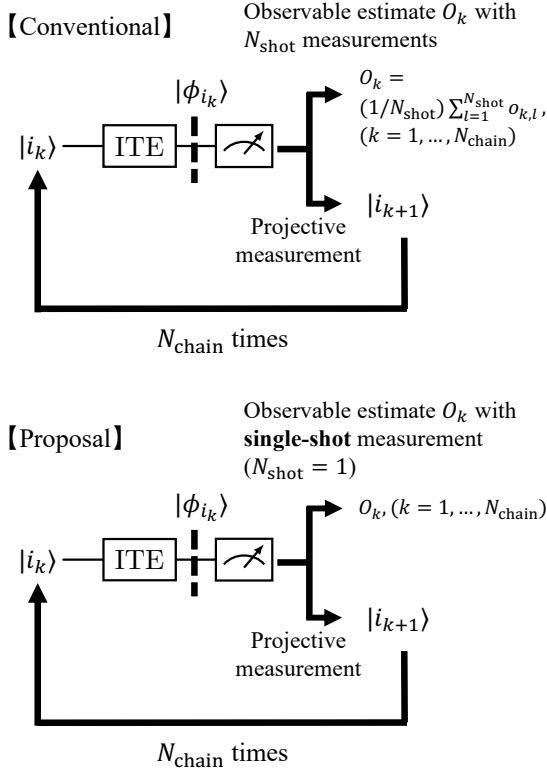


FIG. 2: Comparison between conventional (Top) and proposed single-shot (Bottom) approaches for the estimation of expectation values in QMETTS. In conventional methods, the total number of circuits for constructing estimator $\bar{O} = (1/N_{\text{chain}}) \sum_{k=1}^{N_{\text{chain}}} O_k$ is $N_{\text{est}} = N_{\text{chain}} N_{\text{shot}}$. On the other hand, our approach takes $N_{\text{est}} = N_{\text{chain}}$.

$\text{Var}_{\text{est}}^{(\text{single})}[\bar{O}]$, is given by

$$\text{Var}_{\text{est}}^{(\text{single})}[\bar{O}] = \frac{2\tau^{(\text{single})}}{N_{\text{est}}} \sigma_{\mu}^2 + \frac{2\tau^{(\text{single})}}{N_{\text{est}}} \sigma_{\text{shot}}^2, \quad (16)$$

where $\tau^{(\text{single})}$ is the integrated auto-correlation time for the single-shot approach. Notably, we can show that $\tau^{(\text{single})} < \tau^{(\text{multi})}$; the details are provided in App. A. Intuitively, this occurs because the additional stochasticity from the shot noise helps to reduce the auto-correlation of the Markov chain samples more rapidly. Therefore, under the fixed N_{est} ,

$$\begin{aligned} & \text{Var}_{\text{est}}^{(\text{multi})}[\bar{O}] - \text{Var}_{\text{est}}^{(\text{single})}[\bar{O}] \\ &= 2 \frac{N_{\text{shot}} \tau^{(\text{multi})} - \tau^{(\text{single})}}{N_{\text{est}}} \sigma_{\mu}^2 \\ & \quad + 2 \frac{\tau^{(\text{multi})} - \tau^{(\text{single})}}{N_{\text{est}}} \sigma_{\text{shot}}^2 \\ & \geq 0. \end{aligned} \quad (17)$$

$$(18)$$

This inequality shows that, for a fixed total number of circuit executions, the single-shot strategy yields a smaller estimator variance under the same measurement budget. Furthermore, we can derive the following relation,

$$\sigma_{\mu}^2 + \sigma_{\text{shot}}^2 = \text{Var}_{\text{chain}}[\mathbb{E}_{\text{shot}}[\bar{O}]] + \mathbb{E}_{\text{chain}}[\text{Var}_{\text{shot}}[\bar{O}]] \quad (19)$$

$$= \sum_i \text{Prob}_i \langle \phi_i | \mathcal{O} | \phi_i \rangle^2 - \left(\sum_i \text{Prob}_i \langle \phi_i | \mathcal{O} | \phi_i \rangle \right)^2 + \sum_i \text{Prob}_i \left(\langle \phi_i | \mathcal{O}^2 | \phi_i \rangle - \langle \phi_i | \mathcal{O} | \phi_i \rangle^2 \right) \quad (20)$$

$$= \sum_i \text{Prob}_i \langle \phi_i | \mathcal{O}^2 | \phi_i \rangle - \left(\sum_i \text{Prob}_i \langle \phi_i | \mathcal{O} | \phi_i \rangle \right)^2 \quad (21)$$

$$= \sigma_{\text{Gibbs}}^2, \quad (22)$$

where σ_{Gibbs}^2 is the variance of the observable under the Gibbs state. Thus, the total variance in our approach is proportional to the Gibbs variance, scaled by the factor $2\tau^{(\text{single})}/N_{\text{est}}$. Therefore, the single-shot strategy achieves the optimal scaling determined by the Gibbs variance while simultaneously reducing the auto-correlation time of the estimator. We adopt this single-shot strategy in the numerical simulations presented below. Note that the costs discussed here pertain only to the estimation of the expectation value; the cost of the projective measurements to obtain new collapse states is N_{chain} and the ITE might require an additional measurement cost in practice.

In the subsequent section, we extend this approach to gauge theories. The above strategy works in ordinary quantum many-body systems [27, 40–42]. In gauge theories, however, we need to preserve gauge-invariance. Starting from an initial state in physical space, the imaginary-time evolved states preserve gauge invariance due to $[H, G_n] = 0$. Nevertheless, generic projective measurements do not respect the gauge constraints and may collapse a physical state into an unphysical one. In the next section, we propose novel measurement bases maintaining gauge symmetries while satisfying Eq. (13) within the physical sector.

IV. QMETTS ALGORITHM FOR \mathbb{Z}_2 GAUGE THEORIES

In this section, we propose a way of obtaining the expectation value $\langle \mathcal{O} \rangle_{\beta, \mu}$ in \mathbb{Z}_2 LGTs using the QMETTS algorithm. The key idea is to construct new measurement bases (1) preserving gauge-invariance and (2) satisfying Eq. (13) within the

physical subspace. We denote such a pair of bases as the Mutually Unbiased Physical Bases (MUPB). They can be formally described as follows:

Definition IV.1 (Mutually Unbiased Physical Bases). Two measurement bases $\{|n^{(1)}\rangle\}$ and $\{|m^{(2)}\rangle\}$ are called Mutually Unbiased Physical Bases if they satisfy the following properties:

1. All states of measurement bases $\{|n^{(1)}\rangle\}$ and $\{|m^{(2)}\rangle\}$ are eigenstates of all Gauss's law operators :

$$G_n |i^{(a)}\rangle = g_n |i^{(a)}\rangle, \quad g_n \in \{\pm 1\}, \quad a = 1, 2. \quad (23)$$

2. Any two physical states $|i^{(1)}\rangle, |j^{(2)}\rangle \in \mathcal{H}_{\text{phys}}$ satisfy the relation of the MUB within physical subspace $\mathcal{H}_{\text{phys}}$:

$$|\langle i^{(1)} | j^{(2)} \rangle|^2 = \frac{1}{d_{\text{phys}}}, \quad (24)$$

where d_{phys} denotes the dimension of the physical subspace $\mathcal{H}_{\text{phys}}$.

If we start with a physical state and employing the MUPB for projective measurements to obtain collapse states, the Markov chain is guaranteed to remain within the physical sector, precluding any collapse into unphysical states.

Since standard measurements in quantum computation are performed in the computational basis, alternative measurement bases must be implemented by designing specific quantum circuits. We explicitly identify one of the MUPB in our \mathbb{Z}_2 LGT setup; the corresponding circuit architectures are illustrated in Fig. 3 and Fig. 4. These circuits are characterized by constant depth and nearest-neighbor interactions, ensuring that the construction scales efficiently for larger systems. We refer to these measurement bases as the physical Z -basis and the physical X -basis, with their respective bases denoted by $\{|e_i^{(Z_{\text{phys}})}\rangle\}$ and $\{|e_i^{(X_{\text{phys}})}\rangle\}$. The circuit for the physical Z -basis consists of Hadamard gates acting on the gauge links. In addition to these Hadamard gates, the physical X -basis circuit incorporates a unitary operator W , defined as,

$$W := V^\dagger H_{L_{\text{KS}}} \cdot \left(\prod_{m=1}^{L_{\text{KS}}-1} \sigma_{m,m+1}^H \right) V, \quad (25)$$

$$V := \left(\prod_{m=1}^{L_{\text{KS}}-2} \text{CNOT}_{f_{m+1}, g_{m,m+1}} \right) \cdot \left(\prod_{m=1}^{L_{\text{KS}}-2} \text{CNOT}_{f_m, g_{m,m+1}} \right) \cdot \left(\prod_{m=1}^{L_{\text{KS}}-1} H_m \right), \quad (26)$$

where $\text{CNOT}_{f_p, g_{q,q+1}}$ denotes a Controlled-NOT gate with control qubit f_p and target qubit $g_{q,q+1}$ and $H_p, \sigma_{p,p+1}^H$ denote Hadamard gates acting on site p , link $(p, p+1)$, respectively. This operator W plays a crucial role in mixing physical states while strictly preserving local gauge symmetries.

To prove that the physical Z - and X -bases satisfy the MUPB conditions, we leverage the stabilizer formalism, a mathematical framework originally developed for quantum error correction [25, 26]. In this formalism, quantum states are characterized as the simultaneous $+1$ eigenstates of a set of operators called stabilizers. Similarly, in our \mathbb{Z}_2 LGT setup, gauge constraints can be represented as commuting operators that select the physical subspace; in other words, physical states are those stabilized by the gauge constraint operators. A key advantage of this perspective is that Pauli operators are mapped to other Pauli operators under conjugation by the Clifford group, allowing the structure of these gauge-stabilizing operators to be efficiently tracked under Clifford transformations. This property, in turn, enables an efficient construction of the MUPB. A detailed proof that the physical Z - and X -bases satisfy the MUPB conditions is provided in App. C.

A. Extension to general dimensions and boundary conditions

In Sec. V, we presented numerical results in our $(1+1)$ -dimensional \mathbb{Z}_2 LGT setup. Although these simulations focus on this specific setting, the construction of the MUPB can be generalized to \mathbb{Z}_2 LGTs in arbitrary dimensions and with general boundary conditions.

For \mathbb{Z}_2 LGTs in a general setup, as in the $(1+1)$ -dimensional case, the Gauss's law operators can be described by products of Pauli operators and mutually commute. The physical Hilbert space is defined as the common $+1$ eigenspace of these operators, $G_n |\psi\rangle = +|\psi\rangle, \quad \forall n$. To construct the MUPB in this general setting, we employ the canonical decomposition theorem for stabilizer groups, which allows us to transform the Gauss's law operators into a set of single-Pauli Z operators. As a result of this decomposition, the qubits can be grouped into fixed qubits under these Pauli Z operators and other qubits independent of these constraints. By applying Hadamard gates to the unconstrained qubits, we can then build the MUPB for \mathbb{Z}_2 LGTs in arbitrary dimensions and with general boundary conditions. The required Clifford circuit for the MUPB can be realized using $\mathcal{O}(N_q^2)$ gates with $\mathcal{O}(\log N_q)$ depth, where N_q denotes the system size. This ensures that the MUPB can be constructed efficiently. Details of

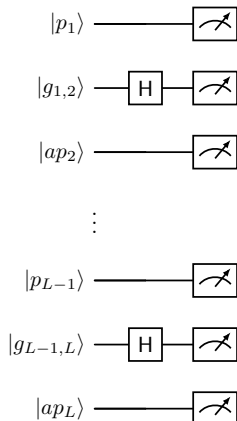


FIG. 3: Quantum circuit for the first measurement basis (physical Z -basis). The circuit illustrates the measurement setup for each qubit, including the link fields $|g_{n-1,n}\rangle$ and matter fields $|p_n\rangle, |ap_n\rangle$.

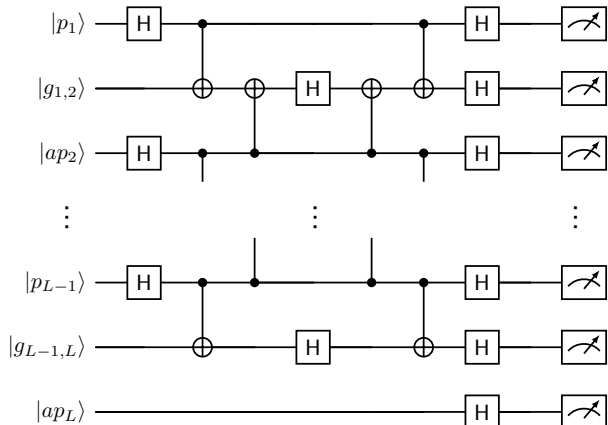


FIG. 4: Quantum circuit for the second measurement basis (physical X -basis). This circuit represents the transformation to a complementary basis using CNOT gates and Hadamard gates.

the construction are provided in App. D.

Since Clifford circuits contain entangling gates such as CNOT, the resulting basis can generate highly entangled states. This feature is particularly beneficial for the QMETTS algorithm, while it is typically difficult to handle within tensor-network-based METTS approaches. Consequently, our construction naturally extends to higher-dimensional systems where tensor-network methods often encounter entanglement bottlenecks.

B. Contribution and relation to prior works

The calculation of thermal equilibrium properties while preserving symmetries has been extensively studied within the framework of the METTS algorithm, particularly for systems with one or a few global conserved quantities by exploiting symmetry-adapted measurement bases in the context of condensed matter.

In Ref. [37], efficient mixing bases are achieved within the METTS framework by employing Fourier-transformed bases and Haar-random bases that respect global symmetries. While these constructions lead to good ergodic properties and short auto-correlations, they typically require high complexity. In contrast, our MUPB approach facilitates efficient mixing using only Clifford gates. Remarkably, these bases can be constructed with constant circuit depth for (1+1)-dimensional systems and $\mathcal{O}(\log N_q)$ depth for higher dimensions, making our method particularly well-suited for near-term quantum devices.

Another related approach was proposed in Ref. [43], where nontrivial measurement bases are generated via time evolution under commuting operators with generators corresponding to symmetries within the METTS framework. This method does not generally guarantee efficient mixing of the Markov chain. Moreover, it remains unclear how this construction can be extended to accommodate local gauge constraints, which impose much more stringent conditions than global symmetries. In contrast, our MUPB framework explicitly ensures both gauge invariance and optimal mixing through a controlled, shallow-depth circuit architecture.

In the present work, we employ the QMETTS framework and introduce measurement bases with substantially lower circuit complexity than those proposed in previous METTS-based studies. While tensor-network approaches face significant challenges in scaling to higher dimensions due to entanglement growth, our measurement bases are intrinsically entangled by the structure of Clifford group and our construction can be easily extended to higher dimensional systems.

V. NUMERICAL RESULTS

In this section, we present numerical results obtained using our algorithm, the QMETTS algorithm using the single-shot approach with the MUPB. We first describe the implementation of the ITE part, which has not been discussed explicitly so far. We then derive the explicit MUPB construction in our \mathbb{Z}_2 LGT setup. Next, we specify the simulation

setup and parameters, and finally provide numerical results, including validation on a small lattice and simulations on larger systems.

A. Imaginary time evolution part

Following previous works, we adopt Quantum Imaginary Time Evolution (QITE) method proposed by Motta et al [21] to implement the ITE process. QITE has been successfully demonstrated in various experimental setups and remains one of the most promising approaches for the NISQ era [44, 45]. However, we emphasize that the QMETTS framework is, in principle, compatible with any imaginary-time evolution algorithm. For instance, recent work has integrated the Adaptive Variational Quantum Imaginary Time Evolution (AVQITE) with the QMETTS algorithm, referred to as the Adaptive Variational QMETTS (AVQMETTS) [46].

To implement the ITE via Trotterization, we decompose the Hamiltonian with chemical potential term into three parts, $H - \mu N = H_e + H_o + H_D$, where

$$\begin{aligned}
H_{e/o} &= -\frac{1}{4a} \sum_{n \in \text{even/odd}}^{L_{\text{KS}}-1} \left[X_n \sigma_{n,n+1}^Z X_{n+1} \right. \\
&\quad \left. + Y_n \sigma_{n,n+1}^Z Y_{n+1} \right], \quad (27) \\
H_D &= ag^2 \sum_{n=1}^{L_{\text{KS}}-1} (1 - \sigma_{n,n+1}^X) + \frac{m}{2} \sum_{n=1}^{L_{\text{KS}}} (-1)^n Z_n \\
&\quad - \frac{\mu}{2} \sum_{n=1}^{L_{\text{KS}}} Z_n. \quad (28)
\end{aligned}$$

As discussed below, this decomposition suppresses Trotter errors. We employ a second-order Trotter decomposition,

$$\begin{aligned}
e^{-\beta(H-\mu N)/2} &= \left(e^{-\Delta\beta(H-\mu N)/2} \right)^{N_s} \\
&\approx \left(\prod_{\gamma \in \{e,o,D\}}^{\leftarrow} \prod_{\gamma \in \{e,o,D\}}^{\rightarrow} e^{-\Delta\beta H_\gamma/4} \right)^{N_s}, \quad (29)
\end{aligned}$$

where $\Delta\beta = \beta/N_s$ and N_s is the number of Trotter steps. The left- and right-ordered products are

defined as

$$\prod_{\gamma \in \{e,o,D\}}^{\leftarrow} e^{-\Delta\beta H_\gamma/4} := e^{-\Delta\beta H_e/4} e^{-\Delta\beta H_o/4} e^{-\Delta\beta H_D/4}, \quad (30)$$

$$\prod_{\gamma \in \{e,o,D\}}^{\rightarrow} e^{-\Delta\beta H_\gamma/4} := e^{-\Delta\beta H_D/4} e^{-\Delta\beta H_o/4} e^{-\Delta\beta H_e/4}. \quad (31)$$

Following Ref. [47], the Trotter error can be bounded in the spectral norm as

$$\begin{aligned}
&\left\| \prod_{\gamma}^{\leftarrow} \prod_{\gamma}^{\rightarrow} e^{-\Delta\beta H_\gamma/4} - e^{-\Delta\beta H} \right\|_{\infty} \\
&= \mathcal{O} \left(\tilde{\alpha}_{\text{comm}}(\Delta\beta)^3 e^{4\Delta\beta \sum_{\gamma} \|H_\gamma\|_{\infty}} \right), \quad (32)
\end{aligned}$$

where $\tilde{\alpha}_{\text{comm}} = \sum_{\gamma_1, \gamma_2, \gamma_3} \|[H_{\gamma_1}, [H_{\gamma_2}, H_{\gamma_3}]]\|_{\infty}$.

Each term H_γ is further decomposed as

$$e^{-\Delta\beta H_\gamma/4} = \prod_m e^{-\Delta\beta h_\gamma[m]/4}, \quad (33)$$

where $H_\gamma = \sum_m h_\gamma[m]$ and each $h_\gamma[m]$ consists of a single Pauli string with a coefficient. Since all $h_\gamma[m]$ within the same H_γ commute, this step introduces no additional Trotter error.

For notational brevity, we denote each elementary operator $e^{-\Delta\beta h_\gamma[m]/4}$ by $e^{-\Delta\tau h}$ in the below discussion. To implement the non-unitary operators $e^{-\Delta\tau h}$, the non-unitary evolution is approximated by a unitary operator $\exp(-i\Delta\tau \sum_I a_I \sigma_I)$, where σ_I are Pauli strings acting on a domain of size D . Those coefficients are determined by minimizing the norm $\|(e^{-i\Delta\tau \sum_I a_I \sigma_I} - e^{-\Delta\tau h})|\Psi\rangle\|$ on classical computers, where $|\Psi\rangle$ is the state before imaginary-time evolution. To achieve good accuracy and make the performance of the QMETTS algorithm clear, in the present work we take full size of domain $D = N_q$, which entails exponential classical cost. Thus, in practice, scalable implementations rely on truncated domains or alternative approaches mentioned in [21, 48].

B. Simulation parameters

Let us explain the parameter setup in our calculations. In our simulations, parameters are rescaled as functions of the gauge coupling g , with $ag = 0.25$ and $m/g = 0.01$. In the case of $L_{\text{KS}} = 2, 4$, the number of qubits required are $N_q = 4, 7$, respectively. For $L_{\text{KS}} = 2$ and 4, we choose the initial states $|0-0\rangle$ and $|0-0+0-0\rangle$ in the qubit description presented in Sec. II, respectively. The number of

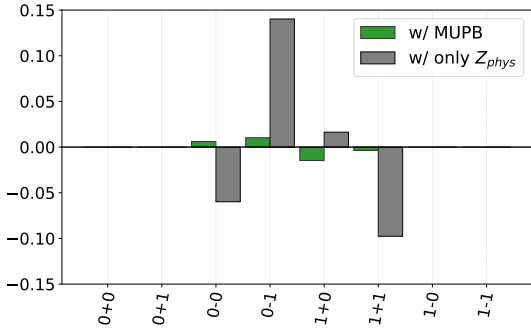


FIG. 5: Deviations of the sampling distributions of the collapse states from the exact stationary distribution,

$\text{Prob}_i = \langle i^{(Z_{\text{phys}})} | e^{-\beta(H-\mu N)} | i^{(Z_{\text{phys}})} \rangle / Z$, are compared for the QMETTS Markov chain using the MUPB (green) and the fixed physical Z -basis (gray). The results are obtained for a system size of $L_{\text{KS}} = 2$ with a total of 1,000 samples in both method at $\beta g = 1.0$. The physical space is spanned by $\mathcal{H}_{\text{phys}} = \text{span}\{|0-0\rangle, |0-1\rangle, |1+0\rangle, |1+1\rangle\}$.

the QMETTS samples is fixed to 1,000, and the imaginary-time step size is set to $\Delta\beta = 0.01$. All numerical simulations were performed using Qiskit.

C. Validation using small lattice setup

To validate the proposed algorithm, we first consider a small lattice with $L_{\text{KS}} = 2$. In this setup, the physical sector is given by $\mathcal{H}_{\text{phys}} = \text{span}\{|0-0\rangle, |0-1\rangle, |1+0\rangle, |1+1\rangle\}$. Figure 5 illustrates the deviations in the physical Z -basis of the sampling distributions of the collapse states from the exact stationary distribution, $\text{Prob}_i = \langle i^{(Z_{\text{phys}})} | e^{-\beta(H-\mu N)} | i^{(Z_{\text{phys}})} \rangle / Z$. Specifically, we compare the results obtained via the MUPB (alternating between physical Z - and X -bases, shown in green) with those obtained by using only the physical Z -basis (shown in gray). As discussed in Sec. III, while both approaches successfully restrict the sampling to the physical sector, which would not be possible using standard, non-gauge-invariant Z - and X -bases, only the MUPB-based QMETTS accurately reproduces the exact stationary distribution. In contrast, the approach restricted to the usage of only the physical Z -basis exhibits significant deviations from the theoretical values. This discrepancy arises because alternating between MUPBs is essential to ensure ergodicity and reduce auto-correlations within the physical subspace. These results confirm that our algorithm correctly samples physical states and faithfully converges to the thermal equilibrium

distribution, thereby validating the proposed framework.

D. Numerical simulation based on proposed algorithm

1. Temperature dependence

We first investigate the temperature dependence of the theory in the zero-density regime using our algorithm. Figures 6(a)–6(c) show the sampling distribution of the collapse states of the physical Z -basis states obtained via the QMETTS algorithm with the MUPB at three representative inverse temperatures: $\beta g = 0.40, 1.00$, and 14.0 . In Fig. 6, all gauge-violating states are grouped into one label “unphysical states”. Consistent with the $L_{\text{KS}} = 2$ case, the samples for $L_{\text{KS}} = 4$ never populate these unphysical states, confirming the strict preservation of gauge invariance. At $\beta = 0.40$ (Fig. 6(a)), the distribution is broad, reflecting strong thermal fluctuations. In contrast, at low temperature ($\beta = 14.0$, Fig. 6(c)), only a small number of collapse states contribute to the distribution. In this regime, since the Gibbs state is well approximated by the ground state, $e^{-\beta(H-\mu N)/2} / Z \approx |\text{G.S.}\rangle \langle \text{G.S.}|$, each sampling distributions of the collapse states should converge to $\propto |\langle i^{(Z_{\text{phys}})} | \text{G.S.}\rangle|^2$, which is the overlap of each collapse state $|i^{(Z_{\text{phys}})}\rangle$ with the ground state. As plotted in Fig. 6(c), the most dominant state is $|1+0+1+0\rangle$, which corresponds to the state with no excitation in the qubit description. This observation indicates that the ground state has primary overlap with no excited state. The next frequent states, including the dimer flux, such as $|0-1+1+0\rangle$ and $|1+0+0-1\rangle$, indicate that the ground state is a quantum superposition of those excitations due to interactions. The empirical distribution derived from the Markov chain samples shows excellent agreement with the exact results, suggesting that the influence of the initial state is negligible. We thus conclude that the Markov chains require no significant burn-in period.

Based on these observations, we plot the β dependence of the energy density $\langle h \rangle_{\beta, \mu} := \langle H \rangle_{\beta, \mu} / L_D$, shown in Fig. 7 incorporating auto-correlations by directly computing the integrated auto-correlation times; see App. B for the detailed numerical analyses. Our results are in agreement with the results of the exact diagonalization (shown in red). Expectation values can be interpreted as the summation of the expectation values under all collapse states, with the probabilities plotted in Fig. 6. At higher temperatures, we observe relatively larger statistical errors compared with low temperature regime;

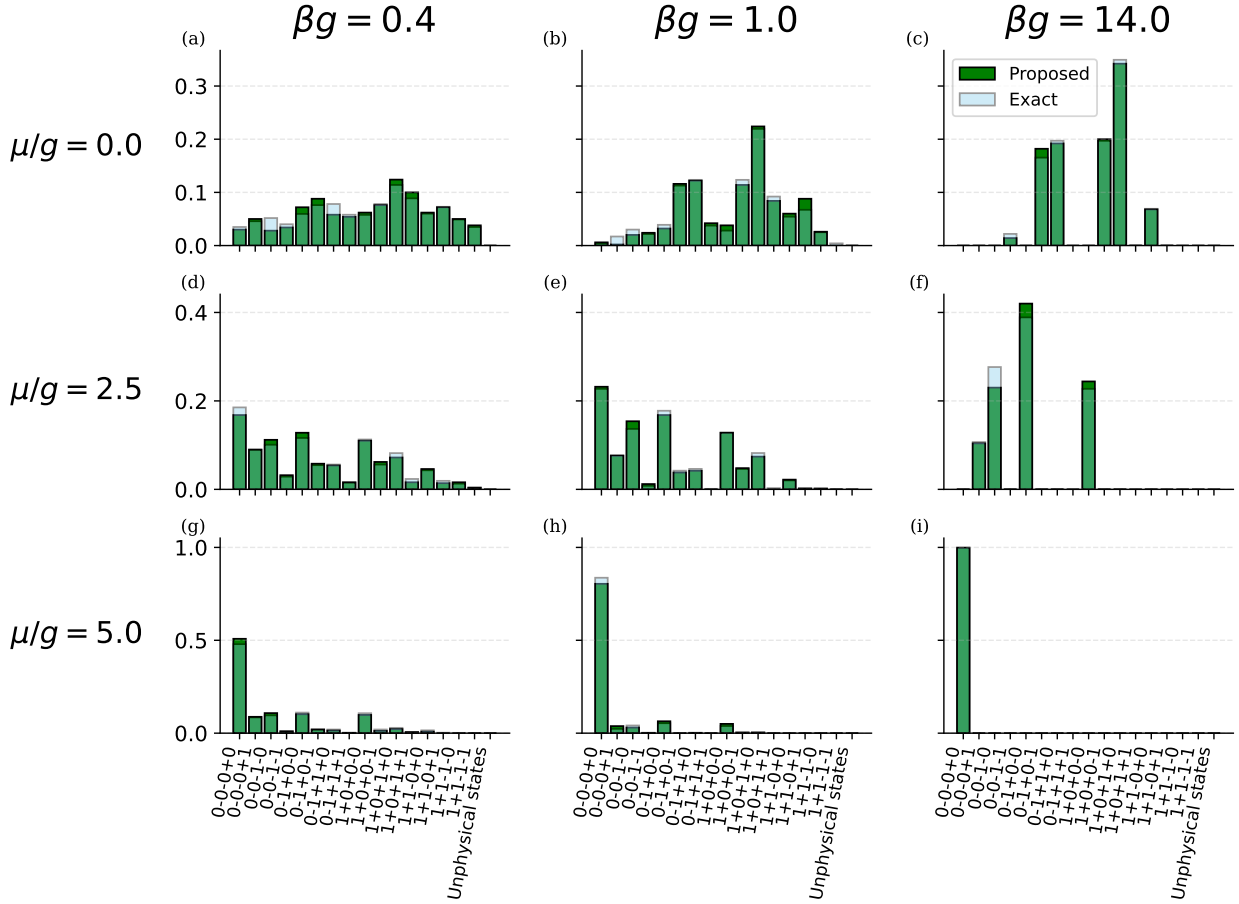


FIG. 6: Sampling distributions of collapse states obtained by the projective measurements during the QMETTS (green) and the exact probabilities (light blue) for $L_{\text{KS}} = 4$. The panels are arranged by chemical potential μ/g (rows) and inverse temperature βg (columns). Top panels (a–c) correspond to $\mu/g = 0.0$, middle panels (d–f) to $\mu/g = 2.5$, and bottom panels (g–i) to $\mu/g = 5.0$. For each row, the columns represent $\beta g = 0.4, 1.0$, and 14.0 , respectively. The exact values are calculated as $\text{Prob}_i = \langle i^{(Z_{\text{phys}})} | e^{-\beta(H - \mu N)} | i^{(Z_{\text{phys}})} \rangle / Z$. All results are obtained with a sample size of 1,000.

see Fig. 7 inset. This is a direct consequence of the broad distribution of frequencies and the large variance of estimator under Gibbs states at high temperature. Since thermal fluctuations require the system to explore a larger portion of the Hilbert space, the variance in the estimator naturally increases.

2. Density dependence

Next, we study the dependence on the chemical potential μ at $\beta = 0.40, 1.00$, and 14.0 . We investigate the sampling distribution of the collapse states varying from $\mu = 0.0$ to $\mu = 2.5, 5.0$, shown in Fig. 6(a) - Fig. 6(i). At high temperature ($\beta = 0.4$), increasing μ suppresses thermal fluctuations; see Fig. 6(a), (d), and (e). At low tempera-

ture ($\beta = 14.0$), the distributions reflect changes of the ground state as a function of μ . In Fig. 6(f) ($\beta = 14.0, \mu = 2.5$), the most dominant state is $|0 - 1 + 0 - 0\rangle$, which corresponds to a configuration with two particle excitations and one anti-particle excitation. In our formulation, the number operator N is defined to yield $+1$ for a particle excitation and -1 for an anti-particle excitation. Thus, this state is an eigenvector of N with an eigenvalue of one ($N = 1$). Notably, all other dominant states in this regime, such as $|1 + 0 + 0 - 0\rangle$, $|0 - 0 - 1 - 0\rangle$, and $|0 - 0 - 0 + 1\rangle$, also possess the eigenvalue $N = 1$, directly reflecting the influence of the chemical potential. In Fig. 6(i), where $\beta g = 14.0, \mu/g = 5.0$, we only observe the state $|0 - 0 - 0 + 0\rangle$, which corresponds to the state where two particles are excited and no anti-particle is. This state have the eigen-

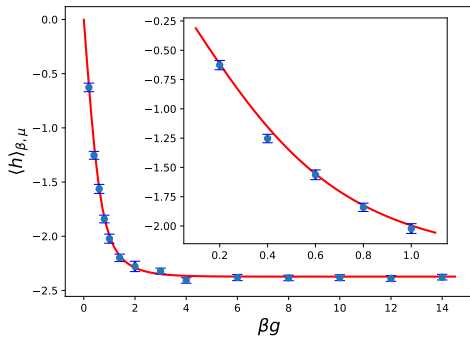


FIG. 7: Temperature dependence of the energy density $\langle h \rangle_{\beta, \mu}$ as a function of inverse temperature βg for $L_{KS} = 4$. The values estimated by the proposed method (blue dots with error bars) are compared with the exact diagonalization results (red line). The inset highlights the high-temperature region $\beta g \in [0, 1.0]$. The statistical errors are observed to be relatively larger in the high-temperature regime compared to the low-temperature regime.

value $N|0-0-0+0\rangle = +2|0-0-0+0\rangle$ and there is no configuration achieving this eigenvalue in our setup.

Based on those distributions, we plot chiral condensate $\langle \bar{\psi}\psi \rangle_{\beta, \mu}$ in Fig. 8(a)-Fig. 8(c). The qubit description of chiral condensate is given by

$$\bar{\psi}\psi := \frac{1}{L_D} \sum_{n=1}^{L_{KS}} (-1)^n \chi_n^\dagger \chi_n = \frac{1}{L_{KS}} \sum_{n=1}^{L_{KS}} (-1)^n Z_n. \quad (34)$$

The chiral condensate is associated with confinement and is expected to vanish in the large- μ limit. Figure 8(a) -Fig. 8(c) show the μ dependence of the chiral condensate at the three temperatures. At $\beta = 14.0$, the restoration of the chiral condensate can be seen at large μ . Especially, high density regime $\mu/g = 5.0$, only the dominant state is only $|0-0-0+0\rangle$ and its expectation values can be computed analytically $\langle \bar{\psi}\psi \rangle_{\beta, \mu} = 0$. Thus, no statistical error is seen in the large μ region. As the temperature increases, this transition is gradually smeared by thermal fluctuations.

We further compute the quark number density $\langle n \rangle_{\beta, \mu} := \langle N \rangle_{\beta, \mu} / L_D$ shown in Fig. 8(d)-Fig. 8(f). The number operator N is defined in Eq. (6). The quark number density represents the occupation number of fermions per site and increases monotonically with μ . Especially, the behavior at $\beta g = 14.0$ reflects the expectation values of the ground states, exhibiting step-like behavior due to the finite lattice size; see Fig. 8(f). In the continuum limit $a \rightarrow 0$,

these steps are expected to smooth out, yielding a continuous curve.

Finally, the phase diagrams presented in Fig. 9 provide a comprehensive view of the $(\mu/g, T/g)$ plane for chiral condensate (left) and quark number density (right). The chiral condensate shows a transition from the broken symmetry phase (dark regions) to the restored phase (light regions) as either temperature or chemical potential increases. The quark number density confirms that the high-density phase coincides with the region of chiral restoration. Notably, the proposed method successfully reproduces these transitions without the sign problem.

VI. CONCLUSION

In this work, we have developed a \mathbb{Z}_2 gauge-invariant framework for computing thermal expectation values by introducing Mutually Unbiased Physical Bases (MUPB) in the QMETTS algorithm. Projective measurements within the MUPB enable us to ensure that the system never collapses into gauge-violating states while reducing the auto-correlation of the Markov chain. By leveraging the mathematical equivalence between \mathbb{Z}_2 lattice gauge theory (LGT) and the stabilizer formalism, we have identified an efficient construction for MUPBs using shallow circuits. This construction is applicable across arbitrary dimensions and boundary conditions. Furthermore, we propose the single-shot approach for the estimation of expectation values, demonstrating that this strategy not only reproduces the exact expectation values but also reduces the variance of the estimators. To validate our methodology, we applied this approach to (1+1)-dimensional \mathbb{Z}_2 LGT, numerically demonstrating that it accurately reproduces thermal properties across a wide range of temperatures and chemical potentials without suffering from sign problems.

Our stabilizer-based construction suggests a straightforward extension to \mathbb{Z}_d , where d is a prime number, lattice gauge theories as d -dimensional qudit systems share an analogous stabilizer structure [49]. On the other hand, extending this framework to continuous or non-Abelian gauge groups remains a non-trivial challenge. For such groups, the existence and construction of MUPB that respect the relevant gauge constraints are not yet established. Addressing these complexities and exploring the applicability of our MUPB framework to these gauge theories will be the focus of future research.

It should be noted that the efficiency of the overall algorithm depends on the performance of the imaginary-time evolution (ITE) scheme. While the QITE method proposed by Motta et al. has been ex-

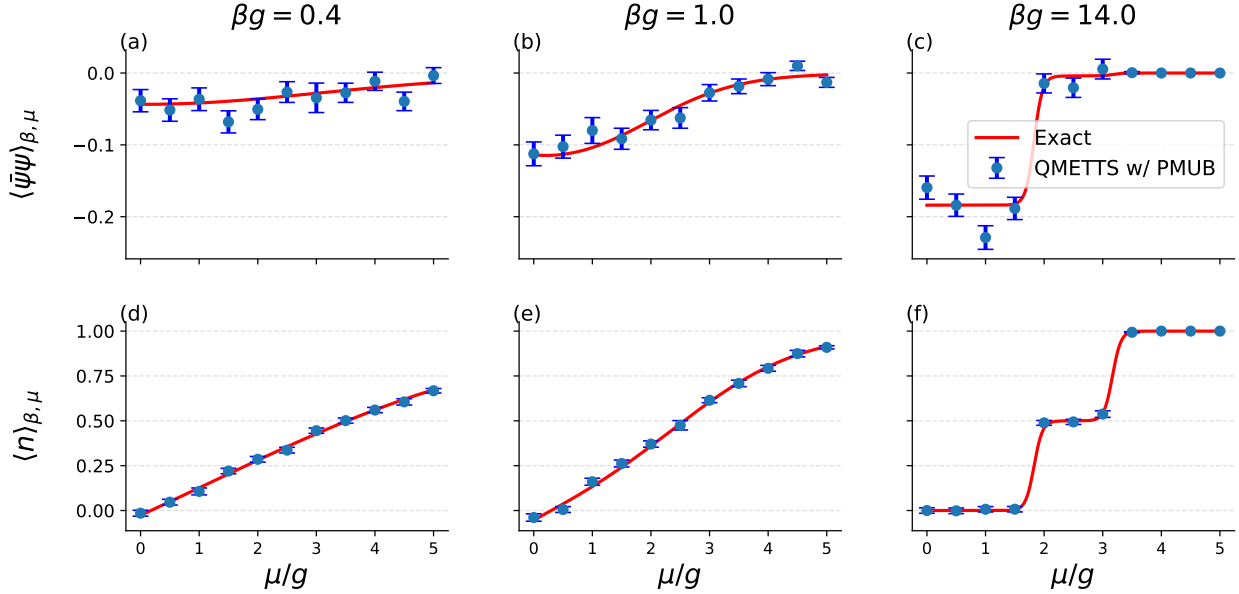


FIG. 8: Dependence of chiral condensate $\langle \bar{\psi}\psi \rangle_{\beta, \mu}$ and quark number density $\langle n \rangle_{\beta, \mu}$ on the chemical potential μ/g for $L_{KS} = 4$. Top panels (a–c) show the chiral condensate, while bottom panels (d–f) show the quark number density. From left to right, the columns correspond to inverse temperatures $\beta g = 0.4$, 1.0 , and 14.0 , respectively. The behavior of $\langle \bar{\psi}\psi \rangle_{\beta, \mu}$ with increasing μ/g reflects the restoration of chiral symmetry at finite density, particularly evident in the sharp transition observed at $\beta g = 14.0$. The exact results are also shown (red line). In the low-temperature limit ($\beta g = 14.0$), the sharp step-like structure in the quark number density is well-reproduced within statistical errors.

perimentally demonstrated in several setups and is suitable for near-term devices, its current implementation may face scalability challenges as the system size increases. To enhance scalability, alternative approaches that circumvent the need for full tomography, such as Probabilistic Imaginary Time Evolution (PITE) [44, 50] or Adiabatic Quantum Imaginary Time Evolution (A-QITE) [51], present promising avenues for future integration.

Finally, our proposed framework is naturally compatible with emerging techniques that leverage gauge symmetry for symmetry verification [52–55]. In such error-mitigation schemes, quantum errors are detected by monitoring violations of gauge constraints, a process that inherently relies on the redundancy of the Hilbert space. Unlike standard approaches that may trace out or eliminate these degrees of freedom, our method explicitly preserves this redundancy, allowing for straightforward integration with symmetry-based error suppression. By combining our MUPB-based QMETTS with these verification protocols, our approach significantly accelerates the realization of practical quantum simulations for lattice gauge theories in the near-term era.

ACKNOWLEDGMENTS

We thank Etsuko Itou, Koji Terashi, and Lento Nagano for discussions and/or comments. We thank Yutaro Iiyama for assistance with numerical calculations. This work was supported by JST SPRING, Grant Number JPMJSP2108.

Appendix A: Auto-correlation

In this appendix, we show that $\tau^{(\text{single})} < \tau^{(\text{multi})}$, where $\tau^{(\text{single})}, \tau^{(\text{multi})}$ are the integrated auto-correlation times with single shot ($N_{\text{shot}} = 1$) and multiple shots per the Markov sample, respectively. For simplicity, we assume that in the multi-shot case, N_{shot} is sufficiently large such that the variance contribution from shot noise is negligible compared to the variance of the Markov chain itself. Under this assumption, we effectively have $\tau^{(\text{multi})} \approx \tau_{\mu}$, where τ_{μ} is the autocorrelation time of the original Markov chain. In the following, we denote $\tau^{(\text{single})}$ as $\tau_{\mathcal{O}}$ for brevity.

The integrated auto-correlation time τ_A ($A =$

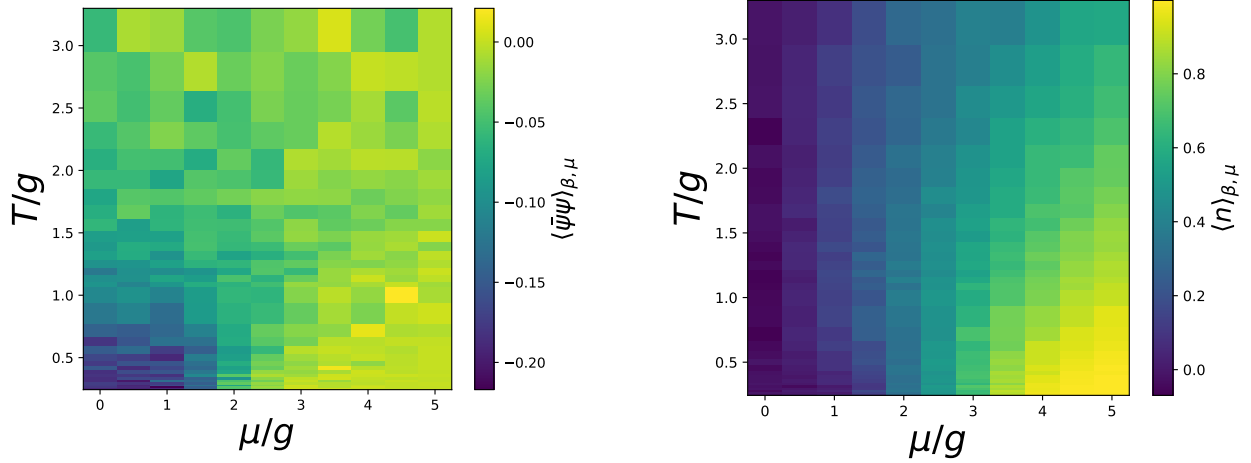


FIG. 9: Phase diagrams in the $(\mu/g, T/g)$ plane for the chiral condensate $\langle\bar{\psi}\psi\rangle_{\beta,\mu}$ (left) and the quark number density $\langle n\rangle_{\beta,\mu}$ (right). The system size is $L_{\text{KS}} = 4$. The color scales indicate the expectation values estimated by the proposed method. The horizontal axis represents the chemical potential μ/g , and the vertical axis represents the temperature T/g .

$\mu, O)$ can be given by

$$\tau_A = \frac{1}{2} + \sum_{t=0}^{\infty} \rho_A(t), \quad (\text{A1})$$

where $\rho_A(t)$ is the autocorrelation function and is given by

$$\rho_A(t) = \frac{\text{Cov}(A_k, A_{k+t})}{\text{Var}(A_k)}. \quad (\text{A2})$$

$\text{Cov}(A_k, A_{k+t})$ is the covariance between A_k and A_{k+t} . Since shot noise ε_k is independent of the Markov chain, the covariance does not change $\text{Cov}(O_k, O_{k+t}) = \text{Cov}(\mu_k, \mu_{k+t})$. On the other hand, the variance of the $\{A_k\}_k$ differs between two cases

$$\text{Var}[\mu_k] = \sigma_\mu^2, \quad (\text{A3})$$

$$\text{Var}[O_k] = \sigma_\mu^2 + \sigma_{\text{shot}}^2. \quad (\text{A4})$$

Consequently, the autocorrelation function for the single-shot observable is rescaled as

$$\rho_O = \frac{\sigma_\mu^2}{\sigma_\mu^2 + \sigma_{\text{shot}}^2} \rho_\mu. \quad (\text{A5})$$

Substituting this into the definition of τ_O , we derive

$$\tau_O = 1 + \alpha(\tau_\mu - 1), \quad (\text{A6})$$

$$\alpha := \frac{\sigma_\mu^2}{\sigma_\mu^2 + \sigma_{\text{shot}}^2}. \quad (\text{A7})$$

Since $\alpha < 1$, we can show that

$$\tau_O = 1 + \alpha(\tau_\mu - 1) < 1 + \tau_\mu - 1 = \tau_\mu. \quad (\text{A8})$$

Appendix B: Numerical results of auto-correlation

In this appendix, we present the numerical results for the integrated auto-correlation time across the $(\mu/g, T/g)$ parameter space. In practice, evaluating the summation in Eq. (A1) in our setup for an infinite chain is impossible and we consider truncated finite chains. To suppress noise from the tail of the autocorrelation function, we introduce a window parameter w to truncate the summation [34]. Under this truncation, the integrated auto-correlation time can be computed by $\tau_A = 1/2 + \sum_{t=0}^w \rho_A(t)$. The top panels of Fig. 10 show the integrated autocorrelation time τ_O for the energy density, chiral condensate, and number density with $w = 10$. We have numerically verified that the results for τ_O are robust against variations in the window size, specifically for $w = 5, 20$, and 40 . The middle panels of Fig. 10 display τ_μ for each observable, while the bottom panels show the deviation $\tau_\mu - \tau_O$. While τ_O remains bounded near $\lesssim 1.0$ across most of the parameter space, τ_μ exceeds ~ 4.0 in certain regions, indicating intrinsic correlations in the chain in spite of the use of the MUPB. As analytically predicted in App. A, we observe $\tau_\mu - \tau_O > 0$ for almost all parameters. Although the sign is occasionally reversed in some regions due to finite chain-length effects and statistical fluctuations in the estimator, the overall trend consistently demonstrates that shot noise effectively reduces the autocorrelation time.

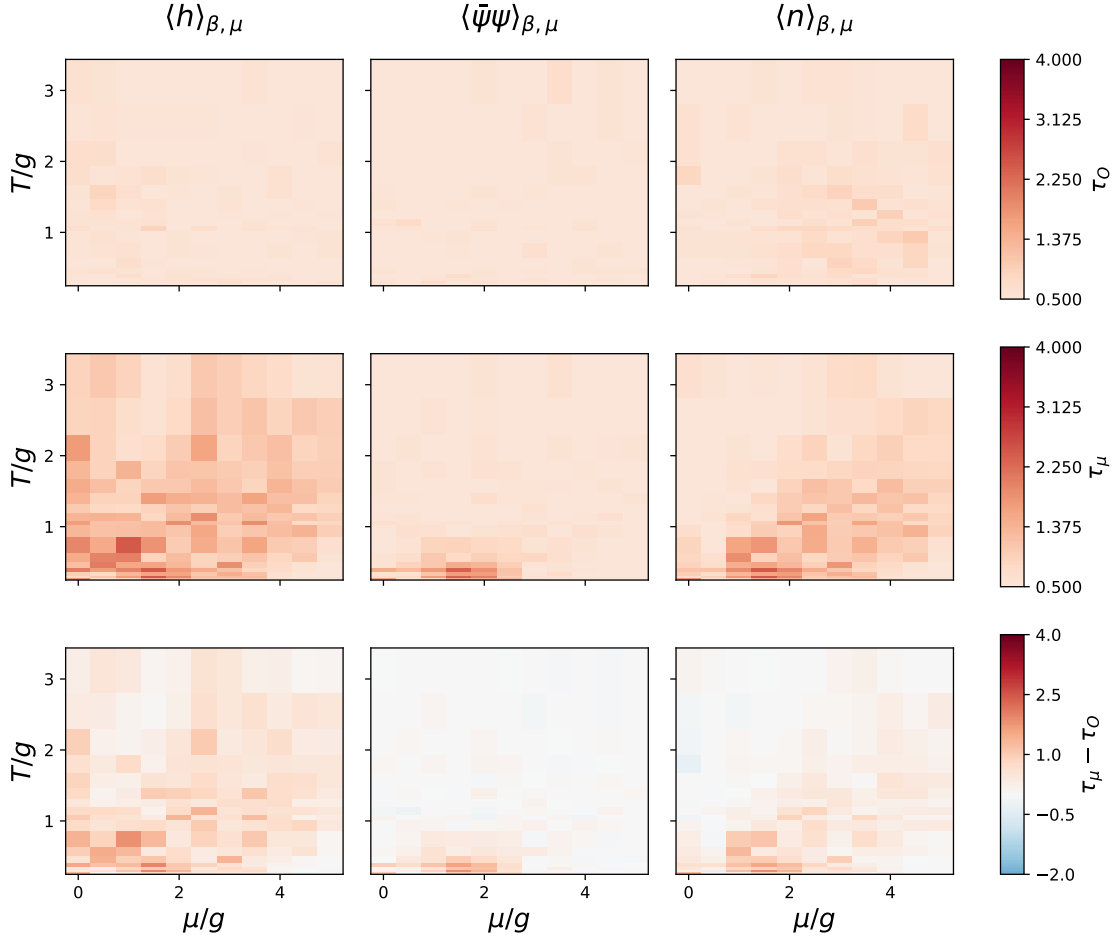


FIG. 10: Integrated auto-correlation times in the Markov chain for energy density, chiral condensate, and number density. Top panels correspond to τ_O , which is the integrated auto-correlation times with single shot for each Markov chain. Middle panels correspond to τ_μ , which is the integrated auto-correlation times without shot noise, representing the genuine Markov chain auto-correlation. Bottom panels show the deviations $\tau_\mu - \tau_O$.

Appendix C: Proof of the Statement

In this section, we provide a formal proof that the physical Z -basis and the physical X -basis, illustrated in Fig. 3 and Fig. 4 respectively, satisfy the conditions for Mutually Unbiased Physical Bases (MUPB) defined through Def. IV.1. Our proof leverages the stabilizer formalism, which is particularly well-suited for describing subspaces defined by symmetry constraints, such as gauge invariance. First, we provide a brief review of the stabilizer formalism. Subsequently, we apply this framework to the \mathbb{Z}_2 lattice gauge theory to rigorously prove our statement.

1. Stabilizer formalism

Let G be group. If a subset $H \subseteq G$ can generate all elements of G through the multiplication of its elements, we refer to H as a generating set of G and denote the group as $G = \langle H \rangle$. The elements of H are called the generators of G . The N -qubit Pauli group is defined as, $\mathcal{P} := \{\pm 1, \pm i\} \otimes \{I, X, Y, Z\}^{\otimes N}$. Stabilizer groups, operators, and states are defined using Pauli group as follows.

Definition C.1. (Stabilizer groups, operators, and states)

A subgroup $\mathcal{S}_N \subseteq \mathcal{P}_N$ is called a stabilizer group if it is Abelian (all elements commute) and does not contain the element $-I$. The elements $S \in \mathcal{S}_N$ are referred to as stabilizer operators. A quantum state

$|\psi\rangle$ is called a stabilizer state of \mathcal{S}_N if it satisfies:

$$S_i |\psi\rangle = + |\psi\rangle \quad \text{for } \forall S_i \in \mathcal{S}_N. \quad (\text{C1})$$

Note that all of stabilizer operators are Hermite and the eigenvalues must be ± 1 since $-I \notin \mathcal{S}_N$. The framework for describing quantum states and subspaces using these groups is known as the stabilizer formalism. The theory of quantum error correction is mainly based on this stabilizer formalism; logical qubits are embedded into space spanned by stabilizer states called code space and errors can be detected by measuring eigenvalues of quantum states.

We also define N -qubit Clifford group which play an important role in describing stabilizer formalism. N -qubit Clifford group \mathcal{C}_N is defined as the normalization group of Pauli group,

$$\mathcal{C}_N := \{C \in \mathcal{U}(\mathbb{C}^2)^{\otimes N} | P \in \mathcal{P}_N, CPC^\dagger \in \mathcal{P}_N\}. \quad (\text{C2})$$

Clifford group consists of Hadamard gates, Phase gates, and CNOT gates. We now summarize some key properties of the stabilizer formalism to provide our proof.

Theorem C.2 ([56]). *Let the system size as N and the number of generators of a stabilizer group \mathcal{S}_N be S . The dimension of the space spanned by the stabilizer group is given by*

$$2^N / 2^S = 2^{N-S}. \quad (\text{C3})$$

Proof. For any non-trivial stabilizer operator $S_i \in \mathcal{S}_N \setminus \{I\}$, its eigenvalues are ± 1 . Since $\text{Tr}[S_i] = 0$ for any Pauli string other than the identity, the multiplicities of the $+1$ and -1 eigenvalues must be equal. Consequently, the projection onto the $+1$ -eigenspace of a single generator S_i bisects the Hilbert space, reducing its dimension by half. Given S independent and commuting generators, each additional generator further constrains the space by a factor of $1/2$. Therefore, the total dimension of the simultaneous $+1$ -eigenspace is 2^{N-S} . \square

Next, we remark the inner product of two stabilizer states $|\phi\rangle$ and $|\psi\rangle$ with different stabilizer groups.

Theorem C.3 ([56]). *Let $|\psi\rangle$ and $|\phi\rangle$ be stabilizer states in an N -qubit system, uniquely determined (up to a global phase) by their respective stabilizer groups $\mathcal{S}_\psi = \{\{P_1, \dots, P_N\}\}$ and $\mathcal{S}_\phi = \{\{Q_1, \dots, Q_N\}\}$. The magnitude of their inner product $|\langle \phi | \psi \rangle|$ is determined as follows,*

1. *If there exists an operator $P \in \mathcal{P}_N$ such that $P \in \mathcal{S}_\psi$ and $-P \in \mathcal{S}_\phi$, the states are orthogonal: $|\langle \phi | \psi \rangle| = 0$.*

Stabilizer formalism	\mathbb{Z}_2 LGTs
Stabilizer operators	Gauss's law operators
Code space	Physical space

TABLE I: Correspondence between the stabilizer formalism and \mathbb{Z}_2 LGTs.

2. *Otherwise, let S be the number of independent generators in \mathcal{S}_ϕ that do not commute with at least one element in \mathcal{S}_ψ . Then, the inner product is given by $|\langle \phi | \psi \rangle| = 2^{-S/2}$.*

Note that the number of different generators cannot be uniquely determined and we must minimize the number of the same generators in step 2.

Proof. First, we prove the first step. If there exists P such that $P|\psi\rangle = |\psi\rangle$ and $-P|\phi\rangle = |\phi\rangle$, $|\psi\rangle$ and $|\phi\rangle$ are in different eigenspaces. Thus, we obtain $\langle \phi | \psi \rangle = 0$.

Next, we prove the second step. By the theorem D.1, there always exists W such that $|\psi\rangle$ transforms into canonical form $W|\psi\rangle = e^{i\theta} |0\rangle^{\otimes N}$, indicating that $W|\psi\rangle$ is stabilized by $\{\{Z_1, \dots, Z_N\}\}$. If we assume that $|\psi\rangle$ and $|\phi\rangle$ have no stabilizer such that the same Pauli string has different signs and the stabilizer groups $\mathcal{S}_W := WS_\phi W^\dagger$, which stabilize the state $W|\phi\rangle$, include only I/Z literals. Then, the inner product of $W|\psi\rangle$ and $W|\phi\rangle$ should be zero from step 1 and it is contradiction. Thus, $W|\psi\rangle$ is stabilized by some X/Y literals, and those literals contribute a factor of $1/\sqrt{2}$ to the inner product. The number of literals X/Y corresponds to the number of different generators, therefore the magnitude of the inner product becomes $|\langle \phi | \psi \rangle| = 2^{-S/2}$ if we have S different generators. \square

Using those properties, we prove our statement in the subsequent section.

2. MUPB Proof

We now apply the stabilizer formalism to rigorously prove that the proposed bases satisfy the condition of the MUPB. First, we remark the mathematical equivalence between the stabilizer formalism and \mathbb{Z}_2 LGT. \mathbb{Z}_2 LGT can be viewed as a stabilizer formalism where the Gauss's law operators serve as the generators of the stabilizer groups. In this perspective, physical states are stabilizer states stabilized by Gauss's law operators, $G_n |\psi\rangle = + |\psi\rangle$. The correspondence is represented in Tab. I. Recently, previous works have been studying this correspondence [52, 57]. By identifying the gauge constraints

as stabilizer generators, we can leverage the theorems established in the previous sections to characterize the physical states.

With these foundations, we now provide the rigorous proof of our main statement. We start to prove that the physical Z -basis and X -basis represented in Fig. 3 and Fig. 4 are eigenstates for Gauss's law operators (Item 1 in Def. IV.1). If we write the measurement bases $\{|e_i^{(Z_{\text{phys}})}\rangle\}_i$ in terms of bit string states $|b_i\rangle = |b_i(1)b_i(2)\dots b_i(N_q)\rangle$, where $b_i(j) \in \{0, 1\}$ means the j -th bit string of the state $|b_i\rangle$, $\{|e_i^{(Z_{\text{phys}})}\rangle\}_i$ is given by

$$|e_i^{(Z_{\text{phys}})}\rangle = \left(\prod_{m=1}^{L_{\text{KS}}-1} \sigma_{m,m+1}^H \right)^\dagger |b_i\rangle =: U_H^\dagger |b_i\rangle. \quad (\text{C4})$$

Since $G_n |e_i^{(Z_{\text{phys}})}\rangle = G_n U_H^\dagger |b_i\rangle = U_H^\dagger \cdot (U_H G_n U_H^\dagger) |b_i\rangle$ and $\sigma_{m-1,m}^H \sigma_{m-1,m}^X \sigma_{m-1,m}^H = \sigma_{m-1,m}^Z$, we obtain

$$U_H G_n U_H^\dagger = (-1)^n \sigma_{n-1,n}^Z Z_n \sigma_{n,n+1}^Z. \quad (\text{C5})$$

As $(-1)^n \sigma_{n-1,n}^Z Z_n \sigma_{n,n+1}^Z |b_i\rangle = z |b_i\rangle$, where $z \in \{\pm 1\}$ is the corresponding eigenvalue, we can show

$$U_H^\dagger \cdot (U_H G_n U_H^\dagger) |b_i\rangle = z U_H^\dagger |b_i\rangle = z |e_i^{(Z_{\text{phys}})}\rangle. \quad (\text{C6})$$

As for $\{|e_i^{(X_{\text{phys}})}\rangle\}$ represented in Fig. 4, since we can describe as $|e_i^{(X_{\text{phys}})}\rangle = W^\dagger |e_i^{(Z_{\text{phys}})}\rangle$,

$$G_n |e_i^{(X_{\text{phys}})}\rangle = G_n W^\dagger |e_i^{(Z_{\text{phys}})}\rangle \quad (\text{C7})$$

$$= W^\dagger (W G_n W^\dagger) |e_i^{(Z_{\text{phys}})}\rangle. \quad (\text{C8})$$

Then,

$$G_n = (-1)^n \sigma_{n-1,n}^X Z_n \sigma_{n,n+1}^X \xrightarrow{V} (-1)^n X_n \quad (\text{C9})$$

$$\xrightarrow{\prod_m \sigma_{m,m+1}^H} (-1)^n X_n \quad (\text{C10})$$

$$\xrightarrow{V^\dagger} (-1)^n \sigma_{n-1,n}^X Z_n \sigma_{n,n+1}^X = G_n, \quad (\text{C11})$$

where $A \xrightarrow{U} B$ denote the conjugation of A under U , $B = U A U^\dagger$. Thus, the Gauss's law operators are invariant under the conjugation $W G_n W^\dagger = G_n$ and we can also prove that $\{|e_i^{(X_{\text{phys}})}\rangle\}$ are eigenstates of G_n .

Next, we try to prove the mutual unbiasedness in physical space: $|\langle e_i^{(Z_{\text{phys}})} | e_j^{(X_{\text{phys}})} \rangle| = 1/\sqrt{d_{\text{inv}}}$ (Item 2 in Def. IV.1). The stabilizer groups which stabilizes $|e_i^{(Z_{\text{phys}})}\rangle$ is given by,

$$\left\{ \{G_n\}_{n=1}^{L_{\text{KS}}-1} \cup \{(-1)^{b_i(g_{n,n+1})} \sigma_{n,n+1}^X\}_{n=1}^{L_{\text{KS}}-1} \cup \{(-1)^{b_i(f_L)} Z_{L_{\text{KS}}}\} \right\}. \quad (\text{C12})$$

From Th. C.2 we can see that the dimension of this stabilized space is $2^0 = 1$ and the state is uniquely determined up to a global phase. Then, the state $|e_i^{(X_{\text{phys}})}\rangle = W^\dagger |e_i^{(Z_{\text{phys}})}\rangle$ can be described by following stabilizer operators through the conjugation under W ,

$$\{(-1)^{b_i(g_{n,n+1})} \sigma_{n,n+1}^X\}_n \xrightarrow{W} \{(-1)^{b_i(g_{n,n+1})} \sigma_{n,n+1}^Z\}_n \cup \{X_{L_{\text{KS}}}\}, \quad (\text{C13})$$

$$\{Z_{L_{\text{KS}}}\} \xrightarrow{W} \{X_{L_{\text{KS}}}\}, \quad (\text{C14})$$

and Gauss's law operators are invariant, $W G_n W^\dagger = G_n$. Since different operators are $\{(-1)^{b_i(g_{n,n+1})} \sigma_{n,n+1}^X\}_{n=1}^{L_{\text{KS}}-1} \cup \{Z_{L_{\text{KS}}}\}$ and $\{(-1)^{b_i(g_{n,n+1})} X_n \sigma_{n,n+1}^Z X_{n+1}\}_{n=1}^{L_{\text{KS}}-1} \cup \{X_{L_{\text{KS}}}\}$, the number of different generators are L_{KS} . Then, by Th. C.3, we can compute the inner product as

$$|\langle e_i^{(Z_{\text{phys}})} | e_j^{(X_{\text{phys}})} \rangle| = \frac{1}{2^{L_{\text{KS}}/2}} = \frac{1}{\sqrt{d_{\text{phys}}}}. \quad (\text{C15})$$

Therefore the physical Z -basis and the physical X -basis satisfy the condition of the MUPB.

Appendix D: General dimension and boundary condition in \mathbb{Z}_2 LGT

Here, we prove that measurement bases satisfying the MUPB condition (Def. IV.1) in arbitrary dimensions and any boundary condition can be constructed with shallow depth quantum circuit, i.e. $\mathcal{O}(\log N)$ depth for the system size N . In this section, we utilize the stabilizer formalism again discussed in App. C. Our concept in this section is mainly based on the literature [56]. First, for the simplicity of the discussion, we introduce the binary expression of the stabilizer formalism. Given N -qubit systems, if we have S generators, stabilizers are represented by $S \times 2N$ matrices, where all elements are 0 or 1, that is $\mathbb{F}_2^{S \times 2N}$. The rows correspond to each stabilizer and the columns to each qubit. The former part of the matrices represents X and the latter Z . Global phases get dropped. For example, Steane five qubit code [25]:

$$XZZXI, IXZZX, XIXZZ, ZXIXZ, \quad (\text{D1})$$

can be equivalently expressed in the following matrix up to global phases:

$$\left(\begin{array}{cccc|cccc} 1 & 0 & 0 & 1 & 0 & 0 & 1 & 1 & 0 & 0 \\ 0 & 1 & 0 & 0 & 1 & 0 & 0 & 1 & 1 & 0 \\ 1 & 0 & 1 & 0 & 0 & 0 & 0 & 0 & 1 & 1 \\ 0 & 1 & 0 & 1 & 0 & 1 & 0 & 0 & 0 & 1 \end{array} \right). \quad (\text{D2})$$

In this expression, $XZZXI$ corresponds to the first row (10010 | 01100). We denote the left (right) space as X (Z) space. In this expression, Clifford gates (Hadamard, Phase, and CNOT) can be interpreted as elementary column operations. Since $HXH = Z$, $HYH = -Y$, Hadamard gates play a role in swapping corresponding two columns. $PZP^\dagger = Z$, $PXP^\dagger = Y$ means that Phase gates P add the columns of X to the columns of Z module 2. $\text{CNOT}_{i,j}$, which controls i -th qubit and acts X gate to j -th qubit, is equivalent with $x_j = x_j \oplus x_i$ and $z_i = z_i \oplus z_j$ since $\text{CNOT}_{i,j}X_j\text{CNOT}_{i,j}^\dagger = X_iX_j$ and $\text{CNOT}_{i,j}Z_i\text{CNOT}_{i,j}^\dagger = Z_iZ_j$, where $x_i(z_i)$ is the i -th column vector and \oplus represents addition modulo 2. Since generators are independent, we can make the matrix in X space has rank S by using H gates. Due to the nature of \mathbb{F}_2 , CNOT gates play a role in adding and swapping column vectors in X space, therefore we can perform Gaussian elimination in X space by using CNOT gates. In addition, commutativity for each generator constraints the space. If the space is represented by $(A|B)$, the commutativity condition is expressed as AB^T to be symmetric.

Based on this expression, we prove the following theorem which is the modified version of the Theorem 8 in the literature [56].

Theorem D.1. *Given any binary matrices $\mathbb{F}_2^{S \times 2N}$, we can transform them into the canonical form by the application of Clifford gates:*

$$(0 \ 0 | I \ 0), \quad (\text{D3})$$

where $I \in \mathbb{F}_2^{S \times S}$.

To prove the above theorem, we show a lemma below.

Lemma D.2 ([56]). *For any symmetric matrix $A \in \mathbb{Z}_2^{n \times n}$, there exists a diagonal matrix Λ such that $A + \Lambda = MM^T$, with M some invertible binary matrix.*

Proof. Let M be a lower-triangular matrix with 1s all along the diagonal:

$$M_{ii} = 1, \quad (\text{D4})$$

$$M_{ij} = 0 \ (i < j). \quad (\text{D5})$$

Such an M is always invertible. If we rewrite the claim in terms of elements,

$$A_{ij} + \Lambda_{ij} = \sum_k M_{ik}M_{jk}, \quad (\text{D6})$$

for all pairs (i, j) . In the case $i = j$, it always holds by taking Λ appropriately. Thus, considering the case $i > j$ is enough since Eq. (D6) is symmetric

under i and j . Hence, we only consider the case $i > j$ below.

Since M is lower-triangular matrix, $M_{ik}M_{jk} = 0$ unless $k \leq j$, following

$$A_{ij} = \sum_{k < j} M_{ik}M_{jk} + M_{ij}. \quad (\text{D7})$$

Based on those observation, we prove we can determine all elements of M by mathematical induction about j .

For $j = 1$, there no exists k such that $k < j = 1$, Eq. (D7) indicates that $A_{i1} = M_{i1}$ for $\forall i (> 1)$. As $M_{11} = 1$, we can determine the elements of M_{i1} for $\forall i$. Next, we assume that $M_{ij'}$ have already been determined for $\forall i$ and $j' < j$. Then, we can obtain M_{ij} from Eq. (D7) because

$$M_{ij} = A_{ij} - \sum_{k < j} M_{ik}M_{jk} \quad (\text{D8})$$

and RHS is already determined from the hypothesis for $j' < j$. \square

Using the above lemma, let us derive the theorem.

Proof. For an arbitrary matrices

$$(A | B), \quad A, B \in \mathbb{F}_2^{S \times N}, \quad (\text{D9})$$

consider following procedures.

1. Use Hadamard gates to make A have rank S .
2. Use CNOTs to perform Gaussian elimination on A , producing

$$(I \ 0 | B) = (I \ 0 | C \ D), \quad (\text{D10})$$

where $C \in \mathbb{F}_2^{S \times S}$ and $D \in \mathbb{F}_2^{S \times (N-S)}$ are the former and latter parts of B .

3. Use Hadamard gates to swap,

$$(I \ D | C \ 0). \quad (\text{D11})$$

4. Again, use CNOTs to perform Gaussian elimination on X space, producing

$$(I \ 0 | C \ 0). \quad (\text{D12})$$

5. Commutativity states that IC^T is symmetric, implying that C is symmetric. We can apply phase gates to add a diagonal matrix to C to convert C into the form $C = MM^T$ for some invertible M based on Lem. D.2.

6. Use CNOTs, producing

$$(M \ 0 | M \ 0). \quad (\text{D13})$$

7. Apply phase gates to S qubits to obtain

$$\left(\begin{array}{cc} M & 0 \\ 0 & 0 \end{array} \right). \quad (\text{D14})$$

8. Again, use CNOTs to perform Gaussian elimination on M , producing

$$\left(\begin{array}{cc} I & 0 \\ 0 & 0 \end{array} \right). \quad (\text{D15})$$

9. Use Hadamard gates for swapping X and Z space

$$\left(\begin{array}{cc} 0 & I \\ I & 0 \end{array} \right). \quad (\text{D16})$$

□

Let us evaluate the circuit complexity in this algorithm. The parallel apply of Hadamard gates and Phase gates implies that step 1, 3, 5, 7, and 9 can be achieved with constant depth and $\mathcal{O}(N)$ gates. Steps 2, 4, 6, and 8 involving CNOTs can be constructed by $\mathcal{O}(N^2)$ gates with $\mathcal{O}(\log N)$ depth for each step based on [58]. In total, we can transform any stabilizer into canonical form using $\mathcal{O}(N^2)$ gates with $\mathcal{O}(\log N)$ depth.

As discussed in App. C, \mathbb{Z}_2 LGTs have the same mathematical structure with the stabilizer formalism. For \mathbb{Z}_2 LGTs in arbitrary dimensions and with general boundary conditions, the gauge groups $\mathcal{G}_N = \langle \{G_n\}_n \rangle$ can be efficiently decomposed using Theorem D.1 followed by the Corollary below.

Corollary D.3. *For any \mathbb{Z}_2 gauge groups \mathcal{G}_N with S independent generators, there exists a element of Clifford group $W \in \mathcal{C}_N$ such that*

$$W\mathcal{G}_N W^\dagger = \{I, Z\}^{\otimes S} \otimes \{I\}^{\otimes N-S} = \langle \{Z_1, Z_2, \dots, Z_S\} \rangle. \quad (\text{D17})$$

W can be constructed using $\mathcal{O}(N^2)$ Hadamard gates, Phase gates, and CNOT gates with $\mathcal{O}(\log N)$ depth.

Based on this corollary, we can derive the efficient quantum circuits to construct the MUPB.

Theorem D.4. *Fig. 11 and Fig. 12 satisfy the condition of the MUPB. W is the element of Clifford group shown in Cor. D.3. W can be constructed using $\mathcal{O}(N^2)$ Hadamard gates, Phase gates and CNOT gates with $\mathcal{O}(\log N)$ depth.*

We denote the measurement bases represented in Figs. 11, 12 by the physical Z -basis and the physical X -basis with their respective basis states denoted by $\{|e_i^{(Z_{\text{phys}})}\rangle\}$ and $\{|e_i^{(X_{\text{phys}})}\rangle\}$ again.

Proof. First, we show that the two measurement bases are eigenstates of Gauss's law operators. The measurement basis in Fig. 11 is given by $|e_i^{(Z_{\text{phys}})}\rangle = W^\dagger |b_i\rangle$, Therefore,

$$G_j |e_i^{(Z_{\text{phys}})}\rangle = W^\dagger (W S_j W^\dagger) |b_i\rangle \quad (\text{D18})$$

$$= z W^\dagger |b_i\rangle \quad (\text{D19})$$

$$= z |e_i^{(Z_{\text{phys}})}\rangle. \quad (\text{D20})$$

Note that $W G_j W^\dagger \in \{I, Z\}^{\otimes S} \otimes \{I\}^{N-S}$. Similarly, we can show

$$G_j |e_i^{(X_{\text{phys}})}\rangle = z |e_i^{(X_{\text{phys}})}\rangle. \quad (\text{D21})$$

Finally, we show the mutually unbiasedness of two measurement bases. By Th. C.2, $d_{\text{inv}} = 2^{N-S}$. A measurement basis state $|e_i^{(Z_{\text{phys}})}\rangle$ is uniquely stabilized by

$$\langle \{G_j\}_{j=1}^S \cup \{W^\dagger (-1)^{b_i(j)} Z_j W\}_{j=S+1}^N \rangle. \quad (\text{D22})$$

On the other hand, a measurement basis $|e_i^{(X_{\text{phys}})}\rangle$ is uniquely stabilized by

$$\langle \{G_j\}_{j=1}^S \cup \{W^\dagger (-1)^{b_i(j)} X_j W\}_{j=S+1}^N \rangle. \quad (\text{D23})$$

Therefore, the number of different stabilizers are $N-S$. Thus,

$$|\langle e_i^{(X_{\text{phys}})} | e_j^{(Z_{\text{phys}})} \rangle| = \frac{1}{2^{(N-S)/2}} = \frac{1}{\sqrt{d_{\text{inv}}}}, \quad (\text{D24})$$

implying that two measurement bases satisfy the condition of the MUPB. □

[1] M. A. Stephanov, "QCD phase diagram: An Overview," *PoS LAT2006* (2006) 024, [arXiv:hep-lat/0701002](#).
 [2] K. Fukushima and T. Hatsuda, "The phase diagram of dense QCD," *Rept. Prog. Phys.* **74** (2011) 014001, [arXiv:1005.4814 \[hep-ph\]](#).
 [3] E. V. Shuryak, "Quantum chromodynamics and the theory of superdense matter," *Physics Reports*

61 no. 2, (1980) 71–158.
 [4] K. G. Wilson, "Confinement of Quarks," *Phys. Rev. D* **10** (1974) 2445–2459.
 [5] J. B. Kogut and L. Susskind, "Hamiltonian Formulation of Wilson's Lattice Gauge Theories," *Phys. Rev. D* **11** (1975) 395–408.
 [6] J. Carlson, S. Gandolfi, F. Pederiva, S. C. Pieper, R. Schiavilla, K. E. Schmidt, and R. B. Wiringa,

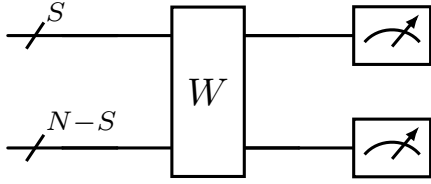


FIG. 11: Quantum circuit for the first measurement basis (physical Z-basis) for any dimension and arbitrary boundary conditions. W is the unitary obtained in Eq. (D17).

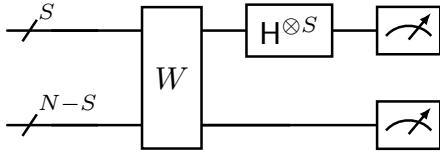


FIG. 12: Quantum circuit for the second measurement basis (physical X-basis) for any dimension and arbitrary boundary conditions. In addition to the apply W , Hadamard gates are applied in the S qubits.

- “Quantum Monte Carlo methods for nuclear physics,” *Rev. Mod. Phys.* **87** (2015) 1067, [arXiv:1412.3081 \[nucl-th\]](#).
- [7] S. Durr, Z. Fodor, J. Frison, C. Hoelbling, R. Hoffmann, S. D. Katz, S. Krieg, T. Kurth, L. Lellouch, T. Lippert, *et al.*, “Ab initio determination of light hadron masses,” *Science* **322** no. 5905, (2008) 1224–1227.
- [8] K. Nagata, “Finite-density lattice QCD and sign problem: Current status and open problems,” *Prog. Part. Nucl. Phys.* **127** (2022) 103991, [arXiv:2108.12423 \[hep-lat\]](#).
- [9] M. Consiglio, J. Settino, A. Giordano, C. Mastroianni, F. Plastina, S. Lorenzo, S. Maniscalco, J. Goold, and T. J. G. Apollaro, “Variational Gibbs state preparation on noisy intermediate-scale quantum devices,” *Phys. Rev. A* **110** no. 1, (2024) 012445, [arXiv:2303.11276 \[quant-ph\]](#).
- [10] T. J. Sewell, C. D. White, and B. Swingle, “Thermal Multi-scale Entanglement Renormalization Ansatz for Variational Gibbs State Preparation,” [arXiv:2210.16419 \[quant-ph\]](#).
- [11] C.-F. Chen, M. J. Kastoryano, and A. Gilyén, “An efficient and exact noncommutative quantum Gibbs sampler,” [arXiv:2311.09207 \[quant-ph\]](#).
- [12] C.-F. Chen, M. J. Kastoryano, F. G. Brandão, and A. Gilyén, “Quantum thermal state preparation,” *arXiv preprint arXiv:2303.18224* (2023).
- [13] D. Zhu, S. Johri, N. M. Linke, K. A. Landsman, N. H. Nguyen, C. H. Alderete, A. Y. Matsuura, T. H. Hsieh, and C. Monroe, “Generation of thermofield double states and critical ground states with a quantum computer,” *Proc. Nat. Acad. Sci.* **117** no. 41, (2020) 25402–25406, [arXiv:1906.02699 \[quant-ph\]](#).
- [14] V. P. Su, “Variational preparation of the thermofield double state of the sachdev-ye-kitaev model,” *Physical Review A* **104** no. 1, (2021) 012427.
- [15] **QuNu** Collaboration, X.-D. Xie, X. Guo, H. Xing, Z.-Y. Xue, D.-B. Zhang, and S.-L. Zhu, “Variational thermal quantum simulation of the lattice Schwinger model,” *Phys. Rev. D* **106** no. 5, (2022) 054509, [arXiv:2205.12767 \[quant-ph\]](#).
- [16] S. Sugiura and A. Shimizu, “Thermal Pure Quantum States at Finite Temperature,” *Phys. Rev. Lett.* **108** (2012) 240401, [arXiv:1112.0740 \[cond-mat.stat-mech\]](#).
- [17] S. Sugiura and A. Shimizu, “Canonical Thermal Pure Quantum State,” *Phys. Rev. Lett.* **111** no. 1, (2013) 010401, [arXiv:1302.3138 \[cond-mat.stat-mech\]](#).
- [18] C. Powers, L. Bassman Oftelie, D. Camps, and W. A. de Jong, “Exploring finite temperature properties of materials with quantum computers,” *Sci. Rep.* **13** no. 1, (2023) 1986, [arXiv:2109.01619 \[quant-ph\]](#).
- [19] L. Coopmans, Y. Kikuchi, and M. Benedetti, “Predicting Gibbs-State Expectation Values with Pure Thermal Shadows,” *PRX Quantum* **4** no. 1, (2023) 010305, [arXiv:2206.05302 \[quant-ph\]](#).
- [20] K. Mizukami and A. Koga, “Quantum algorithm for the microcanonical Thermal Pure Quantum method,” [arXiv:2209.10199 \[quant-ph\]](#).
- [21] M. Motta, C. Sun, A. T. K. Tan, M. J. O. Rourke, E. Ye, A. J. Minnich, F. G. S. L. Brandão, and G. K.-L. Chan, “Determining eigenstates and thermal states on a quantum computer using quantum imaginary time evolution,” *Nature Phys.* **16** (2019) 205–210, [arXiv:1901.07653 \[quant-ph\]](#).
- [22] S. R. White and E. M. Stoudenmire, “Minimally entangled typical thermal state algorithms,” *New J. Phys.* **12** no. 5, (2010) 055026.
- [23] S. R. White, “Minimally entangled typical quantum states at finite temperature,” *Physical review letters* **102** no. 19, (2009) 190601.
- [24] J. Preskill, “Quantum Computing in the NISQ era and beyond,” *Quantum* **2** (2018) 79, [arXiv:1801.00862 \[quant-ph\]](#).
- [25] M. A. Nielsen and I. L. Chuang, *Quantum computation and quantum information*. Cambridge university press, 2010.
- [26] D. Gottesman, “Stabilizer codes and quantum error correction,” [arXiv:quant-ph/9705052](#).
- [27] I.-C. Chen, J. C. Getelina, K. Pollock, A. Khindanov, S. Sen, Y.-X. Yao, and T. Iadecola, “Classical and quantum simulations of 1+1-dimensional \mathbb{Z}_2 gauge theory at finite temperature and density,” *Commun. Phys.* **8**

- no. 1, (2025) 375, [arXiv:2407.11949 \[quant-ph\]](#).
- [28] A. Tomiya, “Schwinger model at finite temperature and density with beta VQE,” [arXiv:2205.08860 \[hep-lat\]](#).
- [29] Z. Davoudi, N. Mueller, and C. Powers, “Towards Quantum Computing Phase Diagrams of Gauge Theories with Thermal Pure Quantum States,” *Phys. Rev. Lett.* **131** no. 8, (2023) 081901, [arXiv:2208.13112 \[hep-lat\]](#).
- [30] D. Horn, M. Weinstein, and S. Yankielowicz, “HAMILTONIAN APPROACH TO Z(N) LATTICE GAUGE THEORIES,” *Phys. Rev. D* **19** (1979) 3715.
- [31] J. Mildenerger, W. Mruczkiewicz, J. C. Halimeh, Z. Jiang, and P. Hauke, “Confinement in a \mathbb{Z}_2 lattice gauge theory on a quantum computer,” *Nature Phys.* **21** no. 2, (2025) 312–317, [arXiv:2203.08905 \[quant-ph\]](#).
- [32] T. Hayata, K. Seki, and A. Yamamoto, “Floquet prethermalization of \mathbb{Z}_2 lattice gauge theory on superconducting qubits,” *Phys. Rev. D* **110** no. 11, (2024) 114503, [arXiv:2408.10079 \[hep-lat\]](#).
- [33] P. Jordan and E. P. Wigner, “About the Pauli exclusion principle,” *Z. Phys.* **47** (1928) 631–651.
- [34] N. Madras and A. D. Sokal, “The pivot algorithm: A highly efficient monte carlo method for the self-avoiding walk,” *Journal of Statistical Physics* **50** no. 1, (1988) 109–186.
- [35] A. Sokal, “Monte carlo methods in statistical mechanics: foundations and new algorithms,” in *Functional integration: Basics and applications*, pp. 131–192. Springer, 1997.
- [36] U. Wolff, A. Collaboration, *et al.*, “Monte carlo errors with less errors,” *Computer Physics Communications* **156** no. 2, (2004) 143–153.
- [37] M. Binder and T. Barthel, “Symmetric minimally entangled typical thermal states for canonical and grand-canonical ensembles,” *Phys. Rev. B* **95** (2017) 195148, [arXiv:1701.03872 \[cond-mat.str-el\]](#).
- [38] B. Bruognolo, J. von Delft, and A. Weichselbaum, “Symmetric minimally entangled typical thermal states,” *arXiv preprint arXiv:1506.03336* (2015).
- [39] W. K. Wootters and B. D. Fields, “Optimal state-determination by mutually unbiased measurements,” *Annals Phys.* **191** no. 2, (1989) 363–381.
- [40] W. Qian and B. Wu, “Quantum computation in fermionic thermal field theories,” *JHEP* **07** (2024) 166, [arXiv:2404.07912 \[hep-ph\]](#).
- [41] A. M. Czajka, Z.-B. Kang, H. Ma, and F. Zhao, “Quantum simulation of chiral phase transitions,” *JHEP* **08** (2022) 209, [arXiv:2112.03944 \[hep-ph\]](#).
- [42] N. Matsumoto, S. Tsutsui, Y. O. Nakagawa, Y. Hidaka, S. Kanasugi, K. Maruyama, H. Oshima, and S. Sato, “Quantum many-body simulation of finite-temperature systems with sampling a series expansion of a quantum imaginary-time evolution,” *Phys. Rev. Res.* **7** no. 1, (2025) 013254, [arXiv:2409.07070 \[quant-ph\]](#).
- [43] S. Goto and I. Danshita, “Quasiexact kondo dynamics of fermionic alkaline-earth-like atoms at finite temperatures,” *Physical Review Letters* **123** no. 14, (2019) 143002.
- [44] H. Nishi, T. Kosugi, and Y.-i. Matsushita, “Implementation of quantum imaginary-time evolution method on NISQ devices by introducing nonlocal approximation,” *npj Quantum Inf.* **7** (2021) 85, [arXiv:2005.12715 \[quant-ph\]](#).
- [45] S.-N. Sun, M. Motta, R. N. Tazhigulov, A. T. K. Tan, G. K.-L. Chan, and A. J. Minnich, “Quantum Computation of Finite-Temperature Static and Dynamical Properties of Spin Systems Using Quantum Imaginary Time Evolution,” *PRX Quantum* **2** no. 1, (2021) 010317, [arXiv:2009.03542 \[quant-ph\]](#).
- [46] J. C. Getelina, N. Gomes, T. Iadecola, P. P. Orth, and Y.-X. Yao, “Adaptive variational quantum minimally entangled typical thermal states for finite temperature simulations,” *SciPost Phys.* **15** no. 3, (2023) 102, [arXiv:2301.02592 \[quant-ph\]](#).
- [47] A. M. Childs, Y. Su, M. C. Tran, N. Wiebe, and S. Zhu, “Theory of trotter error with commutator scaling,” *Physical Review X* **11** no. 1, (2021) 011020.
- [48] N. Gomes, F. Zhang, N. F. Berthussen, C.-Z. Wang, K.-M. Ho, P. P. Orth, and Y. Yao, “Efficient step-merged quantum imaginary time evolution algorithm for quantum chemistry,” *Journal of Chemical Theory and Computation* **16** no. 10, (2020) 6256–6266.
- [49] N. de Beaudrap, “A linearized stabilizer formalism for systems of finite dimension,” *Quant. Inf. Comput.* **13** no. 1-2, (2013) 0073–0115, [arXiv:1102.3354 \[quant-ph\]](#).
- [50] T. Kosugi, Y. Nishiya, H. Nishi, and Y.-i. Matsushita, “Imaginary-time evolution using forward and backward real-time evolution with a single ancilla: First-quantized eigensolver algorithm for quantum chemistry,” *Phys. Rev. Res.* **4** no. 3, (2022) 033121, [arXiv:2111.12471 \[quant-ph\]](#).
- [51] K. Hejazi, M. Motta, and G. K.-L. Chan, “Adiabatic quantum imaginary time evolution,” *Phys. Rev. Res.* **6** no. 3, (2024) 033084, [arXiv:2308.03292 \[quant-ph\]](#).
- [52] T. Schmale and H. Weimer, “Stabilizing quantum simulations of lattice gauge theories by dissipation,” *Phys. Rev. Res.* **6** no. 3, (2024) 033306, [arXiv:2404.16454 \[quant-ph\]](#).
- [53] E. Ballini, J. Mildenerger, M. M. Wauters, and P. Hauke, “Symmetry verification for noisy quantum simulations of non-Abelian lattice gauge theories,” *Quantum* **9** (2025) 1802, [arXiv:2412.07844 \[quant-ph\]](#).
- [54] A. Rajput, A. Roggero, and N. Wiebe, “Quantum error correction with gauge symmetries,” *npj Quantum Inf.* **9** no. 1, (2023) 41, [arXiv:2112.05186 \[quant-ph\]](#).
- [55] M. Carena, H. Lamm, Y.-Y. Li, and W. Liu, “Quantum error thresholds for gauge-redundant

- digitizations of lattice field theories,” *Phys. Rev. D* **110** no. 5, (2024) 054516, [arXiv:2402.16780](#) [hep-lat].
- [56] S. Aaronson and D. Gottesman, “Improved simulation of stabilizer circuits,” *Phys. Rev. A* **70** no. 5, (2004) 052328, [arXiv:quant-ph/0406196](#).
- [57] J. Haruna, “Note on Logical Gates by Gauge Field Formalism of Quantum Error Correction,” [arXiv:2511.15224](#) [hep-th].
- [58] C. Moore and M. Nilsson, “Parallel Quantum Computation and Quantum Codes,” *SIAM J. Comput.* **31** no. 3, (2012) 799–815, [arXiv:quant-ph/9808027](#).